Water: from clouds to planets

Ewine F. van Dishoeck
Leiden Observatory, Leiden University, The Netherlands; Max Planck Institute for Extraterrestrial Physics, Garching, Germany

Edwin A. Bergin
University of Michigan, USA

Dariusz C. Lis
California Institute of Technology, USA

Jonathan I. Lunine
Cornell University, USA

Results from recent space missions, in particular *Spitzer* and *Herschel*, have lead to significant progress in our understanding of the formation and transport of water from clouds to disks, planetesimals, and planets. In this review, we provide the underpinnings for the basic molecular physics and chemistry of water and outline these advances in the context of water formation in space, its transport to a forming disk, its evolution in the disk, and finally the delivery to forming terrestrial worlds and accretion by gas giants. Throughout, we pay close attention to the disposition of water as vapor or solid and whether it might be subject to processing at any stage. The context of the water in the solar system and the isotopic ratios (D/H) in various bodies are discussed as grounding data point for this evolution. Additional advances include growing knowledge of the composition of atmospheres of extra-solar gas giants, which may be influenced by the variable phases of water in the protoplanetary disk. Further, the architecture of extra-solar systems leaves strong hints of dynamical interactions, which are important for the delivery of water and subsequent evolution of planetary systems. We conclude with an exploration of water on Earth and note that all of the processes and key parameters identified here should also hold for exoplanetary systems.

1. INTRODUCTION

With nearly 1000 exoplanets discovered to date and statistics indicating that every star hosts at least one planet (*Batalha et al.*, 2013), the next step in our search for life elsewhere in the universe is to characterize these planets. The presence of water on a planet is universally accepted as essential for its potential habitability. Water in gaseous form acts as a coolant that allows interstellar gas clouds to collapse to form stars, whereas water ice facilitates the sticking of small dust particles that eventually must grow to planetesimals and planets. The development of life requires liquid water and even the most primitive cellular life on Earth consists primarily of water. Water assists many chemical reactions leading to complexity by acting as an effective solvent. It shapes the geology and climate on rocky planets, and is a major or primary constituent of the solid bodies of the outer solar system.

How common are planets that contain water, and how does the water content depend on the planet's formation history and other properties of the star-planet system? Thanks to a number of recent space missions, culminating with the *Herschel Space Observatory*, an enormous step forward has been made in our understanding of where water is formed in space, what its abundance is in various physical environments, and how it is transported from collapsing clouds to forming planetary systems. At the same time, new results are emerging on the water content of bodies in our own solar system and in the atmospheres of known exoplanets. This review attempts to synthesize the results from these different fields by summarizing our current understanding of the water trail from clouds to planets.

Speculations about the presence of water on Mars and other planets in our solar system date back many centuries. Water is firmly detected as gas in the atmospheres of all planets including Mercury and as ice on the surfaces of the terrestrial planets, the Moon, several moons of giant planets, asteroids, comets and Kuiper Belt Objects (see review by *Encrenaz*, 2008). Evidence for past liquid water on Mars has been strengthened by recent data from the Curiosity rover (*Williams et al.*, 2013). Water has also been detected in spectra of the Sun (*Wallace et al.*, 1995) and those of other cool stars. In interstellar space, gaseous water was detected more than 40 years ago in the Orion nebula through its masing transition at 22 GHz (1 cm; *Cheung et al.*, 1969) and water ice was discovered a few years later through its infrared bands toward protostars (*Gillett and Forrest*, 1973).

Water vapor and ice have now been observed in many star- and planet-forming regions throughout the galaxy (reviews by *Cernicharo and Crovisier*, 2005; *Boogert et al.*, 2008; *Melnick*, 2009; *Bergin and van Dishoeck*, 2012) and even in external galaxies out to high redshifts (e.g., *Shimonishi et al.*, 2010; *Lis et al.*, 2011; *Weiß et al.*, 2013). Water is indeed ubiquitous throughout the universe.

On their journey from clouds to cores, the water molecules encounter a wide range of conditions, with temperatures ranging from $<$10 K in cold prestellar cores to $\sim$2000 K in shocks and the inner regions of protoplanetary disks. Densities vary from $\sim 10^4$ cm^{-3} in molecular clouds to 10^{13} cm^{-3} in the midplanes of disks and 10^{19} cm^{-3} in planetary atmospheres. The chemistry naturally responds to these changing conditions. A major question addressed here is to what extent the water molecules produced in interstellar clouds are preserved all the way to exoplanetary atmospheres, or whether water is produced in situ in planet-forming regions. Understanding how, where and when water forms is critical for answering the question whether water-containing planets are common.

2. H_2O PHYSICS AND CHEMISTRY

This section reviews the basic physical and chemical properties of water in its various forms, as relevant for interstellar and planetary system conditions. More details, examples and links to databases can be found in the recent review by *van Dishoeck et al.* (2013).

2.1. Water phases

Water can exist as a gas (vapor or 'steam'), as a solid (ice), or as a liquid. At the low pressures of interstellar space, only water vapor and ice occur, with the temperature at which the transition occurs depending on density. At typical cloud densities of 10^4 particles cm^{-3}, water sublimates around 100 K (*Fraser et al.*, 2001), but at densities of 10^{13} cm^{-3}, corresponding to the midplanes of protoplanetary disks, the sublimation temperature increases to $\sim$160 K. According to the phase diagram of water, liquid water can exist above the triple point at 273 K and 6.12 mbar ($\sim 10^{17}$ cm^{-3}). Such pressures and temperatures are typically achieved at the surfaces of bodies of the size of Mars or larger and at distances between 0.7 and 1.7 AU for a solar-type star.

Water ice can take many different crystalline and amorphous forms depending on temperature and pressure. At interstellar densities, crystallization of an initially amorphous ice to the cubic configuration, I_c, occurs around 90 K. This phase change is irreversible: even when the ice is cooled down again, the crystal structure remains and it therefore provides a record of the temperature history of the ice. Below 90 K, interstellar ice is mostly in a compact high-density amorphous (HDA) phase, which does not naturally occur on planetary surfaces (*Jenniskens and Blake*, 1994). The densities of water ice in the HDA, LDA and I_c phases are 1.17, 0.94 and 0.92 gr cm^{-3}, respectively, much lower than those of rocks (3.2–4.4 gr cm^{-3} for magnesium-iron silicates).

Clathrate hydrates are crystalline water-based solids in which small non-polar molecules can be trapped inside 'cages' of the hydrogen-bonded water molecules. They can be formed when a gas of water mixed with other species condenses[1] out at high pressure and has enough entropy to form a stable clathrate structure (*Lunine and Stevenson*, 1985; *Mousis et al.*, 2010). Clathrate hydrates are found in large quantities on Earth, with methane clathrates on the deep ocean floor and in permafrost as the best known examples. They have been postulated to occur in large quantities on other planets and icy solar system bodies.

2.2. Water spectroscopy

Except for in-situ mass spectroscopy in planetary and cometary atmospheres, all information about interstellar and solar system water comes from spectroscopic data obtained with telescopes. Because of the high abundance of water in the Earth's atmosphere, the bulk of the data comes from space observatories. Like any molecule, water has electronic, vibrational and rotational energy levels. Dipole-allowed transitions between electronic states occur at ultraviolet (UV) wavelengths, between vibrational states at near- to mid-infrared (IR) wavelengths, and between rotational states from mid- to far-IR and submillimeter wavelengths.

Interstellar water vapor observations target mostly the pure rotational transitions. H_2O is an asymmetric rotor with a highly irregular set of energy levels, characterized by quantum numbers $J_{K_A K_C}$. Because water is a light molecule, the spacing of its rotational energy levels is much larger than that of heavy rotors, such as CO or CS, and the corresponding wavelengths much shorter (0.5 mm vs 3–7 mm for the lowest transitions). The nuclear spins of the two hydrogen atoms can be either parallel or anti-parallel, and this results in a grouping of the H_2O energy levels into ortho ($K_A + K_C$ =odd) and para ($K_A + K_C$ =even) ladders, with a statistical weight ratio of 3:1, respectively. Radiative transitions between these two ladders are forbidden to high order, and only chemical reactions in which an H atom of water is exchanged with an H-atom of a reactant can transform ortho- to para-H_2O and vice versa.

Infrared spectroscopy can reveal both water vapor and ice. Water has three active vibrational modes: the fundamental v=1–0 bands of the ν_1 and ν_3 symmetric and asymmetric stretches centered at 2.7 μm and 2.65 μm, respectively, and the ν_2 bending mode at 6.2 μm. Overtone ($\Delta v = 2$ or larger) and combination (e.g., ν_2+ν_3) transitions occur in hot gas at shorter wavelengths (see Fig. 1 for example). Gas-phase water therefore has a rich vibration-rotation spectrum with many individual lines depending on the temperature of the gas. In contrast, the vibrational bands of water ice have no rotational substructure and consist of

[1] Strictly speaking, the term condensation refers to the gas to liquid transition; we adopt here the astronomical parlance where it is also used to denote the gas-to-solid transition.

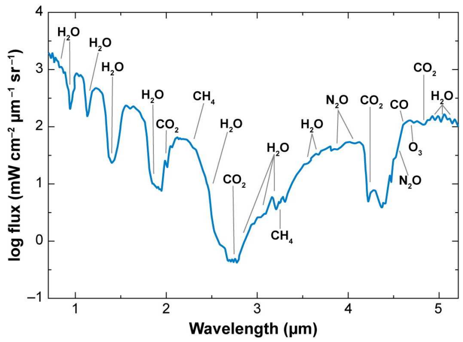

Fig. 1.— The near-IR spectrum of the Earth showing the many water vibrational bands together with CO_2. The bands below 3 μm are due to overtones and combination bands and are often targeted in exoplanet searches. This spectrum was observed with the NIMS instrument on the Galileo spacecraft during its Earth flyby in December 1990. From *Encrenaz* (2008), with permission from Annual Reviews, based on *Drossart et al.* (1993).

very broad profiles, with the much stronger ν_3 band overwhelming the weak ν_1 band. The ice profile shapes depend on the morphology, temperature and environment of the water molecules (*Hudgins et al.*, 1993). Crystalline water ice is readily distinguished by a sharp feature around 3.1 μm that is lacking in amorphous water ice. Libration modes of crystalline water ice are found at 45 and 63 μm (*Moore and Hudson*, 1994).

Spectra of hydrous silicates (also known as phyllosilicates, layer-lattice silicates or ‘clays’) show sharp features at 2.70–2.75 μm due to isolated OH groups and a broader absorption from 2.75–3.2 μm caused by interlayered (‘bound’) water molecules. At longer wavelengths, various peaks can occur depending on the composition; for example, the hydrous silicate montmorillonite has bands at 49 and 100 μm (*Koike et al.*, 1982).

Bound-bound electronic transitions of water occur at far-UV wavelengths around 1240 Å, but have not yet been detected in space.

2.3. Water excitation

The strength of an emission or absorption line of water depends on the number of molecules in the telescope beam and, for gaseous water, on the populations of the individual energy levels. These populations, in turn, are determined by the balance between the collisional and radiative excitation and de-excitation of the levels. The radiative processes involve both spontaneous emission and stimulated absorption and emission by a radiation field produced by a nearby star, by warm dust, or by the molecules themselves.

The main collisional partner in interstellar clouds is H_2. Accurate state-to-state collisional rate coefficients, $C_{u\ell}$, of H_2O with both ortho- and para-H_2 over a wide range of temperatures have recently become available thanks to a dedicated chemical physics study (*Daniel et al.*, 2011). Other collision partners such as H, He and electrons are generally less important. In cometary atmospheres, water itself provides most of the collisional excitation.

Astronomers traditionally analyze molecular observations through a Boltzmann diagram, in which the level populations are plotted versus the energy of the level involved. The slope of the diagram gives the inverse of the excitation temperature. If collisional processes dominate over radiative processes, the populations are in ‘local thermodynamic equilibrium’ (LTE) and the excitation temperature is equal to the kinetic temperature of the gas, $T_{\rm ex} = T_{\rm kin}$. Generally level populations are far from LTE and molecules are excited by collisions and de-excited by spontaneous emission, leading to $T_{\rm ex} < T_{\rm kin}$. The critical density roughly delineates the transition between these regimes: $n_{cr} = A_{u\ell}/C_{u\ell}$ and therefore scales with $\mu_{u\ell}^2 \nu_{u\ell}^3$, where A is the Einstein spontaneous emission coefficient, μ the electric dipole moment and ν the frequency of the transition $u \rightarrow \ell$. In the case of water, the combination of a large dipole moment (1.86 Debye) and high frequencies results in high critical densities of 10^8–10^9 cm^{-3} for pure rotational transitions.

Analysis of water lines is much more complex than for simple molecules, such as CO, for a variety of reasons. First, because of the large dipole moment and high frequencies, the rotational transitions of water are usually highly optically thick, even for abundances as low as 10^{-10}. Second, the water transitions couple effectively with mid- and far-infrared radiation from warm dust, which can pump higher energy levels. Third, the fact that the ‘backbone’ levels with K_A=0 or 1 have lower radiative decay rates than higher K_A levels can lead to population ‘inversion’, in which the population in the upper state divided by its statistical weight exceeds that for the lower state (i.e., $T_{\rm ex}$ becomes negative). Infrared pumping can also initiate this inversion. The result is the well-known maser phenomenon, which is widely observed in several water transitions in star-forming regions (e.g., *Furuya et al.*, 2003; *Neufeld et al.*, 2013; *Hollenbach et al.*, 2013). The bottom line is that accurate analysis of interstellar water spectra often requires additional independent constraints, for example from $H_2^{18}O$ or $H_2^{17}O$ isotopologues, whose abundances are reduced by factors of about 550 and 2500, respectively, and whose lines are more optically thin. At infrared wavelengths, lines are often spectrally unresolved, which further hinders the interpretation.

2.4. Water chemistry

2.4.1. Elemental abundances and equilibrium chemistry

The overall abundance of elemental oxygen with respect to total hydrogen nuclei in the interstellar medium is estimated to be 5.75×10^{-4} (*Przybilla et al.*, 2008), of which 16–24% is locked up in refractory silicate material in the diffuse interstellar medium (*Whittet*, 2010). The abundance of volatile oxygen (i.e., not tied up in some refractory form) is measured to be 3.2×10^{-4} in diffuse clouds (*Meyer et al.*, 1998), so this is the maximum amount of oxygen that can

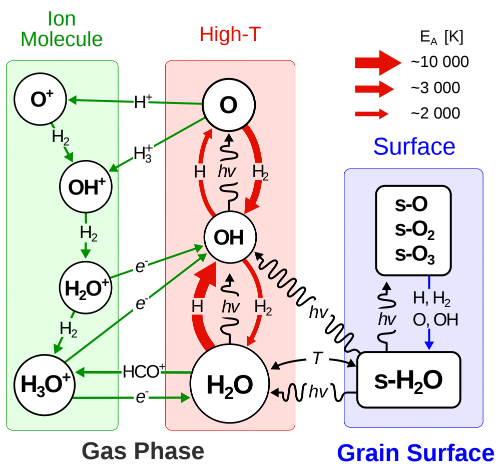

Fig. 2.— Summary of the main gas-phase and solid-state chemical reactions leading to the formation and destruction of H_2O under non-equilibrium conditions. Three different chemical regimes can be distinguished: (i) ion-molecule chemistry, which dominates gas-phase chemistry at low T; (ii) high-temperature neutral-neutral chemistry; and (iii) solid state chemistry. e stands for electron, ν for photon and $s{-}$X indicates that species X is on the grains. Simplified version of figure by *van Dishoeck et al.* (2011).

cycle between water vapor and ice in dense clouds. Counting up all the forms of detected oxygen in diffuse clouds, the sum is less than the overall elemental oxygen abudance. Thus, a fraction of oxygen is postulated to be in some yet unknown refractory form, called UDO ('unknown depleted oxygen'), whose fraction may increase from 20% in diffuse clouds up to 50% in dense star-forming regions (*Whittet*, 2010). For comparison, the abundances of elemental carbon and nitrogen are 3×10^{-4} and 1×10^{-4}, respectively, with about 2/3 of the carbon thought to be locked up in solid carbonaceous material.

For a gas in thermodynamic equilibrium (TE), the fractional abundance of water is simply determined by the elemental composition of the gas and the stabilities of the molecules and solids that can be produced from it. For standard interstellar abundances[2] with [O]/[C]$>$ 1, there are two molecules in which oxygen can be locked up: CO and H_2O. At high pressures in TE, the fraction of CO results from the equilibrium between CO and CH_4, with CO favored at higher temperatures. For the volatile elemental abundances quoted above, this results in an H_2O fractional abundance of $(2-3) \times 10^{-4}$ with respect to total hydrogen, if the CO fractional abundance ranges from $(0-1) \times 10^{-4}$. With respect to H_2, the water abundance would then be $(5-6) \times 10^{-4}$ assuming that the fraction of hydrogen in atomic form is negligible (the density of hydrogen nuclei $n_{\rm H} = n({\rm H}) + 2n({\rm H_2})$). Equilibrium chemistry is established at densities above roughly 10^{13} cm^{-3}, when three body processes become significant. Such conditions are found in planetary atmospheres and in the shielded midplanes of the inner few AU of protoplanetary disks.

Under most conditions in interstellar space, however, the densities are too low for equilibrium chemistry to be established. Also, strong UV irradiation drives the chemistry out of equilibrium, even in high-density environments, such as the upper atmospheres of planets and disks. Under these conditions, the fractional abundances are determined by the kinetics of the two-body reactions between the various species in the gas. Figure 2 summarizes the three routes to water formation that have been identified. Each of these routes dominates in a specific environment.

2.4.2. *Low temperature gas-phase chemistry*

In diffuse and translucent interstellar clouds with densities less than $\sim 10^4$ cm^{-3} and temperatures below 100 K, water is formed largely by a series of ion-molecule reactions (e.g., *Herbst and Klemperer*, 1973). The network starts with the reactions O + H_3^+ and O^+ + H_2 leading to OH^+. The H_3^+ ion is produced by interactions of energetic cosmic-ray particles with the gas, producing H_2^+ and H^+, with the subsequent fast reaction of $H_2^+ + H_2$ leading to H_3^+. The cosmic ray ionization rate of atomic hydrogen denoted by $\zeta_{\rm H}$ can be as high as 10^{-15} s^{-1} in some diffuse clouds, but drops to 10^{-17} s^{-1} in denser regions (*Indriolo and McCall*, 2012; *Rimmer et al.*, 2012). The ionization rate of H_2 is $\zeta_{\rm H_2} \approx 2\zeta_{\rm H}$.

A series of rapid reactions of OH^+ and H_2O^+ with H_2 lead to H_3O^+, which can dissociatively recombine to form H_2O and OH with branching ratios of $\sim$0.17 and 0.83, respectively (*Buhr et al.*, 2010). H_2O is destroyed by photodissociation and by reactions with C^+, H_3^+ and other ions such as HCO^+. Photodissociation of H_2O starts to be effective shortward of 1800 Å and continues down to the ionization threshold at 983 Å (12.61 eV), including Ly α at 1216 Å. Its lifetime in the general interstellar radiation field, as given by *Draine* (1978), is only 40 yr.

2.4.3. *High-temperature gas-phase chemistry*

At temperatures above 230 K, the energy barriers for reactions with H_2 can be overcome and the reaction O + H_2 $\rightarrow$ OH + H becomes the dominant channel initiating water formation (*Elitzur and Watson*, 1978). OH subsequently reacts with H_2 to form H_2O, a reaction which is exothermic, but has an energy barrier of $\sim$2100 K (*Atkinson et al.*, 2004). This route drives all the available gas-phase oxygen into H_2O, unless strong UV or a high atomic H abundance convert some water back to OH and O. High-temperature chemistry dominates the formation of water in shocks, in the inner envelopes around protostars, and in the warm surface layers of protoplanetary disks.

[2] The notation [X] indicates the overall abundance of element X in all forms, be it atoms, molecules or solids.

2.4.4. *Ice chemistry*

The timescale for an atom or molecule to collide with a grain and stick to it is $t_{\rm fo} = 3 \times 10^9/n_{\rm H_2}$ yr for normal size grains and sticking probabilities close to unity (*Hollenbach et al.*, 2009). Thus, for densities greater than 10^4 cm^{-3}, the time scales for freeze-out are less than a few $\times 10^5$ yr, generally smaller than the lifetime of dense cores (at least 10^5 yr). Reactions involving dust grains are therefore an integral part of the chemistry. Even weakly bound species, such as atomic H, have a long enough residence time on the grains at temperatures of 10–20 K to react; H_2 also participates in some surface reactions, but remains largely in the gas. *Tielens and Hagen* (1982) postulated that the formation of water from O atoms proceeds through three routes involving hydrogenation of s-O, s-O_2 and s-O_3, respectively, where s-X indicates a species on the surface. All three routes have recently been verified and quantified in the laboratory and detailed networks with simulations have been drawn up (see *Cuppen et al.*, 2010; *Oba et al.*, 2012; *Lamberts et al.*, 2013, for summaries).

Water ice formation is in competition with various desorption processes, which limit the ice build-up. At dust temperatures below the thermal sublimation limit, photodesorption is an effective mechanism to get species back to the gas phase, although only a small fraction of the UV absorptions results in desorption of intact H_2O molecules (*Andersson and van Dishoeck*, 2008). The efficiency is about 10^{-3} per incident photon, as determined through laboratory experiments and theory (*Westley et al.*, 1995; *Öberg et al.*, 2009; *Arasa et al.*, 2010). Only the top few monolayers of the ice contribute. The UV needed to trigger photodesorption can come either from a nearby star, or from the general interstellar radiation field. Deep inside clouds, cosmic rays produce a low level of UV flux, $\sim 10^4$ photons cm^{-2} s^{-1}, through interaction with H_2 (*Prasad and Tarafdar*, 1983). Photodesorption via X-rays is judged to be inefficient, although there are large uncertainties in the transfer of heat within a porous aggregate (*Najita et al.*, 2001). UV photodesorption of ice is thought to dominate the production of gaseous water in cold pre-stellar cores, the cold outer envelopes of protostars and the outer parts of protoplanetary disks.

Other non-thermal ice desorption processes include cosmic ray induced spot heating (which works for CO, but is generally not efficient for strongly bound molecules like H_2O) and desorption due to the energy liberated by the reaction (called 'reactive' or 'chemical' desorption). These processes are less well explored than photodesorption, but a recent laboratory study of s-D + s-OD $\rightarrow$ s-D_2O suggests that as much as 90% of the product can be released into the gas phase (*Dulieu et al.*, 2013). The details of this mechanism, which has not yet been included in models, are not yet understood and may strongly depend on the substrate.

Once the dust temperature rises above $\sim$100 K (precise value being pressure dependent), H_2O ice thermally sublimates on timescales of years, leading to initial gas-phase abundances of H_2O as high as the original ice abundances. These simulations use a binding energy of 5600 K for amorphous ice and a slightly higher value of 5770 K for crystalline ice, derived from laboratory experiments (*Fraser et al.*, 2001). Thermal desorption of ices contributes to the gas-phase water abundance in the warm inner protostellar envelopes ('hot cores') and inside the snow line in disks.

2.4.5. *Water deuteration*

Deuterated water, HDO and D_2O, is formed through the same processes as illustrated in Figure 2. There are, however, a number of chemical processes that can enhance the HDO/H_2O and D_2O/H_2O ratios by orders of magnitude compared with the overall [D]/[H] ratio of 2.0×10^{-5} in the local interstellar medium (*Prodanović et al.*, 2010). A detailed description is given in the chapter by *Ceccarelli et al.*, here only a brief summary is provided.

In terms of pure gas-phase chemistry, the direct exchange reaction H_2O +HD $\leftrightarrow$ HDO + H_2 is often considered in solar system models (*Richet et al.*, 1977). In thermochemical equilibrium this reaction can provide at most a factor of 3 enhancement, and even that may be limited by kinetics (*Lécluse and Robert*, 1994). The exchange reaction D + OH $\rightarrow$ H + OD, which has a barrier of $\sim$100 K (*Sultanov and Balakrishnan*, 2004), is particularly effective in high-temperature gas such as present in the inner disk (*Thi et al.*, 2010b). Photodissociation of HDO enhances OD compared with OH by a factor of 2–3, which could be a route to further fractionation.

The bulk of the deuterium fractionation in cold clouds comes from gas-grain processes. *Tielens* (1983) pointed out that the fraction of deuterium relative to hydrogen atoms arriving on a grain surface, D/H, is much higher than the overall [D]/[H] ratio, which can be implanted into molecules in the ice. This naturally leads to enhanced formation of OD, HDO and D_2O ice according to the grain-surface formation routes. The high atomic D/H ratio in the gas arises from the enhanced gaseous H_2D^+, HD_2^+, and D_3^+ abundances at low temperatures ($\leq$25 K), when the ortho-H_2 abundance drops and their main destroyer, CO, freezes out on the grains (*Pagani et al.*, 1992; *Roberts et al.*, 2003). Dissociative recombination with electrons then produces enhanced D. The enhanced H_2D^+ also leads to enhanced H_2DO^+ and thus HDO in cold gas, but this is usually a minor route compared with gas-grain processes.

On the grains, tunneling reactions can have the opposite effect, reducing the deuterium fractionation. For example, the OD + H_2 tunneling reaction producing HDO ice is expected to occur slower than the OH + H_2 reaction leading to H_2O ice. On the other hand, thermal exchange reactions in the ice, such as H_2O + OD $\rightarrow$ HDO + OH have been shown to occur rapidly in ices at higher temperatures; these can both enhance and decrease the fractionation. Both thermal desorption at high ice temperatures and photodesorption at low ice temperatures have a negligible effect on the deuterium fractionation, i.e., the gaseous HDO/H_2O and

D_2O/H_2O ratios reflect the ice ratios if no other gas-phase processes are involved.

3. CLOUDS AND PRE-STELLAR CORES: ONSET OF WATER FORMATION

In this and following sections, our knowledge of the water reservoirs during the various evolutionary stages from clouds to planets will be discussed. The focus is on low-mass protostars ($<$100 $L_{\odot}$) and pre-main sequence stars (spectral type A or later). Unless stated otherwise, fractional abundances are quoted with respect to H_2 and are simply called 'abundances'. Often the denominator, i.e., the (column) density of H_2, is more uncertain than the numerator.

The bulk of the water in space is formed on the surfaces of dust grains in dense molecular clouds. Although a small amount of water is produced in the gas in diffuse molecular clouds through ion-molecule chemistry, its abundance of $\sim 10^{-8}$ found by *Herschel*-HIFI (*Flagey et al.*, 2013) is negligible compared with that produced in the solid state. In contrast, observations of the 3 μm water ice band toward numerous infrared sources behind molecular clouds, from the ground and from space, show that water ice formation starts at a threshold extinction of $A_V \approx 3$ mag (*Whittet et al.*, 2013). These clouds have densities of at least 1000 cm^{-3}, but are not yet collapsing to form stars. The ice abundance is s-$H_2O/H_2 \approx 5 \times 10^{-5}$, indicating that a significant fraction of the available oxygen has been transformed to water ice even at this early stage (*Whittet et al.*, 1988; *Murakawa et al.*, 2000; *Boogert et al.*, 2011). Such high ice abundances are too large to result from freeze-out of gas-phase water produced by ion-molecule reactions.

The densest cold cores just prior to collapse have such high extinctions that direct IR ice observations are not possible. In contrast, the water reservoir (gas plus ice) can be inferred from *Herschel*-HIFI observations of such cores. Fig. 3 presents the detection of the H_2O 1_{10}–1_{01} 557 GHz line toward L1544 (*Caselli et al.*, 2012). The line shows blue-shifted emission and red-shifted absorption, indicative of inward motions in the core. Because of the high critical density of water, the emission indicates that water vapor must be present in the dense central part. The infalling red-shifted gas originates on the near-side. Because the different parts of the line profile probe different parts of the core, the line shape can be used to reconstruct the water vapor abundance as a function of position throughout the entire core.

The best-fit water abundance profile is obtained with a simple gas-grain model, in which atomic O is converted into water ice on the grains, with only a small fraction returned back into the gas by photodesorption (*Bergin et al.*, 2000; *Roberts and Herbst*, 2002; *Hollenbach et al.*, 2009). The maximum gas-phase water abundance of $\sim 10^{-7}$ occurs in a ring at the edge of the core around $A_V \approx 4$ mag, where external UV photons can still penetrate to photodesorb the ice, but where they are no longer effective in photodissociating the water vapor. In the central shielded part of the core, cosmic ray induced UV photons keep a small, $\sim 10^{-9}$, but measurable fraction of water in the gas (*Caselli et al.*, 2012). Quantitatively, the models indicate that the bulk of the available oxygen has been transformed into water ice in the core, with an ice abundance of $\sim 10^{-4}$ with respect to H_2.

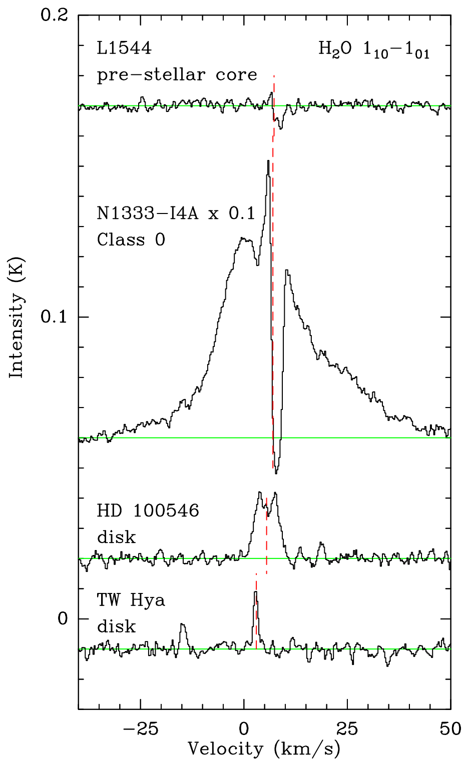

Fig. 3.— *Herschel*-HIFI spectra of the H_2O 1_{10}–1_{01} line at 557 GHz in a pre-stellar core (top), protostellar envelope (middle) and two protoplanetary disks (bottom) (spectra shifted vertically for clarity). The red dashed line indicates the rest velocity of the source. Note the different scales: water vapor emission is strong toward protostars, but very weak in cold cores and disks. The feature at -15 km s^{-1} in the TW Hya spectrum is due to NH_3. Figure by L. Kristensen, adapted from *Caselli et al.* (2012), *Kristensen et al.* (2012) and *Hogerheijde et al.* (2011, and in prep.).

4. PROTOSTARS AND OUTFLOWS

4.1. Outflows

Herschel-HIFI and PACS data show strong and broad water profiles characteristic of shocks associated with embedded protostars, from low to high mass. In fact, for low-mass protostars this shocked water emission completely overwhelms the narrower lines from the bulk of the collapsing envelope, even though the shocks contain less than 1% of the mass of the system. Maps of the water emission around solar-mass protostars such as L1157 reveal water not only at the protostellar position but also along the out-

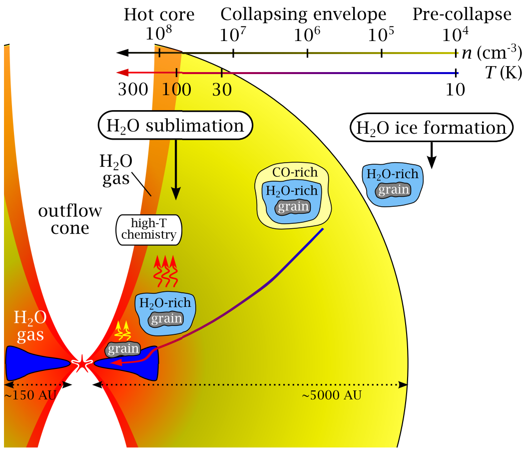

Fig. 4.— Schematic representation of a protostellar envelope and embedded disk with key steps in the water chemistry indicated. Water ice is formed in the parent cloud before collapse and stays mostly as ice until the ice sublimation temperature of $\sim$100 K close to the protostar is reached. Hot water is formed in high abundances in shocks associated with the outflow, but this water is not incorporated into the planet-forming disk. Figure by R. Visser, adapted from *Herbst and van Dishoeck* (2009).

flow at 'hot spots' where the precessing jet interacts with the cloud (*Nisini et al.*, 2010). Thus, water traces the *currently* shocked gas at positions, which are somewhat offset from the bulk of the cooler entrained outflow gas seen in the red- and blue-shifted lobes of low-J CO lines (*Tafalla et al.*, 2013; *Lefloch et al.*, 2010).

Determinations of the water abundance in shocks vary from values as low as 10^{-7} to as high as 10^{-4} (see *van Dishoeck et al.*, 2013, for summary). In non-dissociative shocks, the temperature reaches values of a few thousand K and all available oxygen is expected to be driven into water (*Kaufman and Neufeld*, 1996). The low values likely point to the importance of UV radiation in the shock chemistry and shock structure. For the purposes of this chapter, the main point is that even though water is rapidly produced in shocks at potentially high abundances, the amount of water contained in the shocks is small, and, moreover, most of it is lost to space through outflows.

4.2. Protostellar envelopes: the cold outer reservoir

As the cloud collapses to form a protostar in the center, the water-ice coated grains created in the natal molecular cloud move inward, feeding the growing star and its surrounding disk (Fig. 4). The water ice abundance can be measured directly through infrared spectroscopy of various water ice bands toward the protostar itself. Close to a hundred sources have been observed, from very low luminosity objects ('proto-brown dwarfs') to the highest mass protostars (*Gibb et al.*, 2004; *Pontoppidan et al.*, 2004; *Boogert et al.*, 2008; *Zasowski et al.*, 2009; *Öberg et al.*, 2011). Inferred ice abundances with respect to H_2 integrated along the line of sight are (0.5–1)$\times10^{-4}$.

The water vapor abundance in protostellar envelopes is probed through spectrally-resolved *Herschel*-HIFI lines. Because the gaseous water line profiles are dominated by broad outflow emission (Fig. 3), this component needs to be subtracted, or an optically thin water isotopologue needs to be used to determine the quiescent water. Clues to the water vapor abundance structure can be obtained through narrow absorption and emission features in so-called (inverse) P-Cygni profiles (see NGC 1333 IRAS 4A in Fig. 3). The analysis of these data proceeds along the same lines as for pre-stellar cores. The main difference is that the dust temperature now increases inwards, from a low value of 10–20 K at the edge to a high value of several hundred K in the center of the core (Fig. 4). In the simplest spherically symmetric case, the density follows a power-law $n \propto r^{-p}$ with p=1–2. As for pre-stellar cores, the data require the presence of a photodesorption layer at the edge of the core with a decreasing water abundance at smaller radii, where gaseous water is maintained by the cosmic ray induced photodesorption of water ice (*Coutens et al.*, 2012; *Mottram et al.*, 2013). Analysis of the combined gaseous water and water ice data for the same source shows that the ice/gas ratio is at least 10^4 (*Boonman and van Dishoeck*, 2003). Thus, the bulk of the water stays in the ice in this cold part, at a high abundance of $\sim 10^{-4}$ as indicated by direct measurements of both the water ice and gas.

4.3. Protostellar envelopes: the warm inner part

When the infalling parcel enters the radius at which the dust temperature reaches $\sim$100 K, the gaseous water abundance jumps from a low value around 10^{-10} to values as high as 10^{-4} (e.g., *Boonman et al.*, 2003; *Herpin et al.*, 2012; *Coutens et al.*, 2012). The 100 K radius scales roughly as $2.3 \times 10^{14} \sqrt{(L/L_\odot)}$ cm (*Bisschop et al.*, 2007), and is small, <100 AU, for low-mass sources and a few thousand AU for high-mass protostars. The precise abundance of water in the warm gas is still uncertain, however, and can range from 10^{-6}–10^{-4} depending on the source and analysis (*Emprechtinger et al.*, 2013; *Visser et al.*, 2013). A high water abundance would indicate that all water sublimates from the grains in the 'hot core' before the material enters the disk; a low abundance the opposite.

The fate of water in protostellar envelopes on scales of the size of the embedded disk is currently not well understood, yet it is a crucial step in the water trail from clouds to disks. To probe the inner few hundred AU, a high excitation line of a water isotopolog line not dominated by the outflow or high angular resolution is needed: ground-based millimeter interferometry of the $H_2^{18}O$ $3_{13} - 2_{20}$ ($E_u = 204$ K) line at 203 GHz (*Persson et al.*, 2012) and deep *Herschel*-HIFI spectra of excited $H_2^{18}O$ or $H_2^{17}O$ lines, such as the $3_{12} - 3_{03}$ ($E_u = 249$ K) line at 1095 GHz have been used. Two main problems need to be faced in the analysis. First, comparison of ground-based and *Herschel* lines for the same source show that the high frequency

HIFI lines can be optically thick even for $H_2{}^{18}O$ and $H_2^{17}O$, because of their much higher Einstein A coefficients. Second, the physical structure of the envelope and embedded disk on scales of a few hundred AU is not well understood (*Jørgensen et al.*, 2005), so that abundances are difficult to determine since the column of warm H_2 is poorly constrained. Compact flattened dust structures are not necessarily disks in Keplerian rotation (*Chiang et al.*, 2008) and only a fraction of this material may be at high temperatures.

Jørgensen and van Dishoeck (2010b) and *Persson et al.* (2012) measure water columns and use H_2 columns derived from continuum interferometry data on the same scales ($\sim$1″) to determine water abundances of $\sim 10^{-8} - 10^{-5}$ for three low-mass protostars, consistent with the fact that the bulk of the gas on these scales is cold and water is frozen. From a combined analysis of the interferometric and HIFI data, using $C^{18}O$ 9–8 and 10–9 data to determine the *warm* H_2 column, *Visser et al.* (2013) infer water abundances of $2 \times 10^{-5} - 2 \times 10^{-4}$ in the $\geq$100 K gas, as expected for the larger-scale hot cores.

The important implication of these results is that the bulk of the water stays as ice in the inner few hundred AU and that only a few % of the dust may be at high enough temperatures to thermally sublimate H_2O . This small fraction of gas passing through high-temperature conditions for ice sublimation is consistent with 2D models of collapsing envelope and disk formation, which give fractions of $< 1 - 20\%$ depending on initial conditions (*Visser et al.*, 2009, 2011; *Ilee et al.*, 2011; *Harsono et al.*, 2013; *Hincelin et al.*, 2013).

4.4. Entering the disk: the accretion shock and history of water in disks

The fact that only a small fraction of the material within a few hundred AU radius is at $\geq$ 100 K (§ 4.3) implies that most of the water is present as ice and is still moving inwards (Fig. 4). At some radius, however, the high-velocity infalling parcels must encounter the low-velocity embedded disk, resulting in a shock at the boundary. This shock results in higher dust temperatures behind the shock front than those achieved by stellar heating (*Neufeld and Hollenbach* 1994; see *Visser et al.* 2009 for a simple fitting formula) and can also sputter ices. At early times, accretion velocities are high and all ices would sublimate or experience a shock strong enough to induce sputtering. However, this material normally ends up in the star rather than in the disk, so it is not of interest for the current story. The bulk of the disk is thought to be made up through layered accretion of parcels that fall in later in the collapse process, and which enter the disk at large radii, where the shock is much weaker (*Visser et al.*, 2009). Indeed, the narrow line widths of $H_2^{18}O$ of only 1 km s^{-1} seen in the interferometric data (*Jørgensen and van Dishoeck*, 2010b) argue against earlier suggestions, based on *Spitzer* data, of large amounts of hot water going through an accretion shock in the embedded phase, or even being created through high-temperature chemistry in such a shock (*Watson et al.*, 2007). This view that accretion shocks do not play a role also contrasts with the traditional view in the solar system community that all ices evaporate and recondense when entering the disk (*Lunine et al.*, 1991; *Owen and Bar-Nun*, 1993).

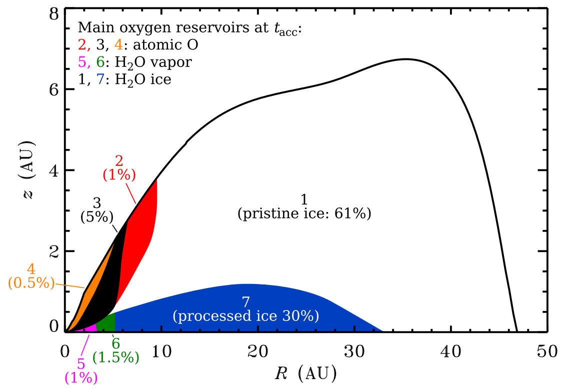

Fig. 5.— Schematic view of the history of H_2O gas and ice throughout a young disk at the end of the accretion phase. The main oxygen reservoir is indicated for each zone. The percentages indicate the fraction of disk mass contained in each zone. Zone 1 contains pristine H_2O formed prior to star formation and never altered during the trajectory from cloud to disk. In Zone 7, the ice has sublimated once and recondensed again. Thus, the ice in planet- and planetesimal-forming zones of disks is a mix of pristine and processed ice. From *Visser et al.* (2011).

Figure 5 shows the history of water molecules in disks at the end of the collapse phase at $t_{acc} = 2.5 \times 10^5$ yr for a standard model with an initial core mass of 1 $M_\odot$, angular momentum $\Omega_0 = 10^{-14}$ s^{-1} and sound speed $c_s = 0.26$ km s^{-1} (*Visser et al.*, 2011). The material ending up in zone 1 is the only water that is completely 'pristine', i.e., formed as ice in the cloud and never sublimated, ending up intact in the disk. Material ending up in the other zones contains water that sublimated at some point along the infalling trajectory. In zones 2, 3 and 4, close to the outflow cavity, most of the oxygen is in atomic form due to photodissociation, with varying degrees of subsequent reformation. In zones 5 and 6, most oxygen is in gaseous water. Material in zone 7 enters the disk early and comes close enough to the star to sublimate. This material does not end up in the star, however, but is transported outward in the disk to conserve angular momentum, re-freezing when the temperature becomes low enough. The detailed chemistry and fractions of water in each of these zones depend on the adopted physical model and on whether vertical mixing is included (*Semenov and Wiebe*, 2011), but the overall picture is robust.

5. PROTOPLANETARY DISKS

Once accretion stops and the envelope has dissipated, a pre-main sequence star is left, surrounded by a disk of gas and dust. These protoplanetary disks form the crucial link between material in clouds and that in planetary systems. Thanks to the new observational facilities, combined with sophisticated disk chemistry models, the various water reservoirs in disks are now starting to be mapped out. Throughout this chapter, we will call the disk out of which our own solar system formed the 'solar nebula disk'. [3]

5.1. Hot and cold water in disks: observations

With increasing wavelengths, regions further out and deeper into the disk can be probed. The surface layers of the inner few AU of disks are probed by near- and mid-IR observations. *Spitzer*-IRS detected a surprising wealth of highly-excited pure rotational lines of warm water at 10–30 μm (*Carr and Najita*, 2008; *Salyk et al.*, 2008), and these lines have since been shown to be ubiquitous in disks around low-mass T Tauri stars (*Pontoppidan et al.*, 2010a; *Salyk et al.*, 2011), with line profiles consistent with a disk origin (*Pontoppidan et al.*, 2010b). Typical water excitation temperatures are $T_{\rm ex}$≈450 K. Spectrally resolved ground-based near-IR vibration-rotation lines around 3 μm show that in some sources the water originates in both a disk and a slow disk wind (*Salyk et al.*, 2008; *Mandell et al.*, 2012). Abundance ratios are difficult to extract from the observations, because the lines are highly saturated and, in the case of *Spitzer* data, spectrally unresolved. Also, the IR lines only probe down to moderate height in the disk until the dust becomes optically thick. Nevertheless, within the more than an order of magnitude uncertainty, abundance ratios of H_2O/CO$\sim$1–10 have been inferred for emitting radii up to a few AU (*Salyk et al.*, 2011; *Mandell et al.*, 2012). This indicates that the inner disks have high water abundances of order $\sim 10^{-4}$ and are thus not dry, at least not in their surface layers. The IR data show a clear dichotomy in H_2O detection rate between disks around the lower-mass T Tauri stars and higher-mass, hotter A-type stars (*Pontoppidan et al.*, 2010a; *Fedele et al.*, 2011). Also, transition disks with inner dust holes show a lack of water line emission. This is likely due to more rapid photodissociation by stars with higher T_*, and thus stronger UV radiation, in regions where the molecules are not shielded by dust.

Moving to longer wavelengths, *Herschel*-PACS spectra probe gas at intermediate radii of the disk, out to 100 AU. Far-IR lines from warm water have been detected in a few disks (*Rivière-Marichalar et al.*, 2012; *Meeus et al.*, 2012; *Fedele et al.*, 2012, 2013). As for the inner disk, the abundance ratios derived from these data are highly uncertain. Sources in which both H_2O and CO far-infrared lines have been detected (only a few) indicate H_2O/CO column density ratios of 10^{-1}, suggesting a water abundance of order 10^{-5} at intermediate layers, but upper limits in other disks suggest values that may be significantly less. Again the disks around T Tauri stars appear to be richer in water than those around A-type stars (Fig. 6).

In principle, the pattern of water lines with wavelength should allow the transition from the gaseous water-rich to

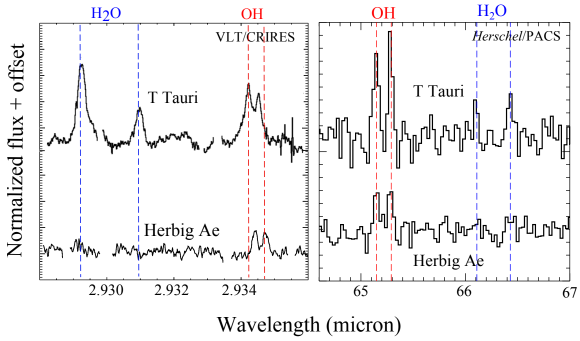

Fig. 6.— Near-IR (left) and far-IR (right) spectra of a T Tau and a Herbig Ae disk, showing OH lines in both but H_2O primarily in disks around cooler T Tau stars. Figure by D. Fedele, based on *Fedele et al.* (2011, 2013).

the water-poor (the snow line) to be probed. As shown by LTE excitation disk models, the largest sensitivity to the location of the snow line is provided by lines in the 40–60 μm region, which is exactly the wavelength range without observational facilities except for SOFIA (*Meijerink et al.*, 2009). For one disk, that around TW Hya, the available shorter and longer wavelength water data have been used to put together a water abundance profile across the entire disk (*Zhang et al.*, 2013). This disk has a dust hole within 4 AU, within which water is found to be depleted. The water abundance rises sharply to a high abundance at the inner edge of the outer disk at 4 AU, but then drops again to very low values as water freezes out in the cold outer disk.

The cold gaseous water reservoir beyond 100 AU is uniquely probed by *Herschel*-HIFI data of the ground rotational transitions at 557 and 1113 GHz. Weak, but clear detections of both lines have been obtained in two disks, around the nearby T Tau star TW Hya (*Hogerheijde et al.*, 2011) and the Herbig Ae star HD 100546 (*Hogerheijde et al.*, in prep.) (Fig. 3). These are the deepest integrations obtained with the HIFI instrument, with integration times up to 25 hr per line. Similarly deep integrations on 5 other disks do not show detections of water at the same level, nor do shallower observations of a dozen other disks of different characteristics. One possible exception, DG Tau (*Podio et al.*, 2013), is a late class I source with a well-known jet and a high X-ray flux. The TW Hya detection implies abundances of gaseous water around 10^{-7} in the intermediate layer of the disk, with the bulk of the oxygen in ice on grains at lower layers. Quantitatively, 0.005 Earth oceans of gaseous water and a few thousand oceans of water ice have been detected (1 Earth ocean = 1.4×10^{24} gr=0.00023 $M_{\rm Earth}$). While this is plenty of water to seed an Earth-like planet with water, a single Jovian-type planet formed in this ice-rich region could lock up the bulk of this water.

Direct detections of water ice are complicated by the fact that IR absorption spectroscopy requires a background light source, and thus a favorable near edge-on orientation of the disk. In addition, care has to be taken that foreground clouds do not contribute to the water ice absorption (*Pon-*

[3] Alternative nomenclatures in the literature include 'primordial disk', 'presolar disk', 'protosolar nebula' or 'primitive solar nebula'.

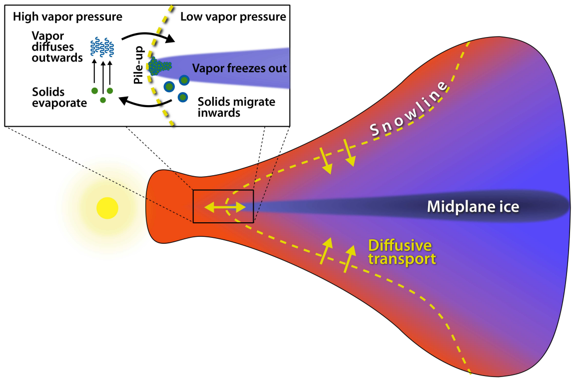

Fig. 7.— Cartoon illustrating the snow line as a function of radius and height in a disk and transport of icy planetesimals across the snowline. Diffusion of water vapor from inner to outer disk followed by freeze-out results in pile-up of ice just beyond the snowline (the cold finger effect). Figure by M. Persson, based on *Meijerink et al.* (2009); *Ciesla and Cuzzi* (2006).

toppidan et al., 2005). The 3 μm water ice band has been detected in only a few disks (*Terada et al.*, 2007; *Honda et al.*, 2009). To measure the bulk of the ice, one needs to go to longer wavelengths, where the ice features can be seen in emission. Indeed, the crystalline H_2O features at 45 or 60 μm have been detected in several sources with ISO-LWS (*Malfait et al.*, 1998, 1999; *Chiang et al.*, 2001) and *Herschel*-PACS (*McClure et al.*, 2012, *Bouwman et al.*, in prep). Quantitatively, the data are consistent with 25–50% of the oxygen in water ice on grains in the emitting layer.

The ISO-LWS far-infrared spectra also suggested a strong signature of hydrated silicates in at least one target (*Malfait et al.*, 1999). Newer *Herschel*-PACS data show no sign of such a feature in the same target (*Bouwman*, priv. comm.). An earlier claim of hydrated silicates at 2.7 μm in diffuse clouds has now also been refuted (*Whittet et al.*, 1998; *Whittet*, 2010). Moreover, there is no convincing detection of any mid-infrared feature of hydrated silicates in hundreds of *Spitzer* spectra of T Tauri (e.g., *Olofsson et al.*, 2009; *Watson et al.*, 2009), Herbig Ae (e.g., *Juhász et al.*, 2010) and warm debris (e.g., *Olofsson et al.*, 2012) disks. Overall, the strong observational consensus is that the silicates prior to planet formation are 'dry'.

5.2. Chemical models of disks

The observations of gaseous water discussed in § 5.1 indicate the presence of both rotationally hot $T_{\rm ex} \approx 450$ K and cold ($T_{\rm ex} < 50$ K) water vapor, with abundances of $\sim 10^{-4}$ and much lower values, respectively. Based on the chemistry of water vapor discussed in § 2.4, we expect it to have a relatively well understood distribution within the framework of the disk thermal structure, potentially modified by motions of the various solid or gaseous reservoirs. This is broadly consistent with the observations.

Traditionally, the snow line plays a critical role in the distribution of water, representing the condensation or sublimation front of water in the disk, where the gas temperatures and pressures allow water to transition between the solid and gaseous states (Fig. 7). For the solar nebula disk, there is a rich literature on the topic (*Hayashi*, 1981; *Sasselov and Lecar*, 2000; *Podolak and Zucker*, 2004; *Lecar et al.*, 2006; *Davis*, 2007; *Dodson-Robinson et al.*, 2009). Within our modern astrophysical understanding, this dividing line in the midplane is altered when viewed within the framework of the entire disk physical structure. There are a number of recent models of the water distribution that elucidate these key issues (*Glassgold et al.*, 2009; *Woitke et al.*, 2009b; *Bethell and Bergin*, 2009; *Willacy and Woods*, 2009; *Gorti et al.*, 2011; *Najita et al.*, 2011; *Vasyunin et al.*, 2011; *Fogel et al.*, 2011; *Walsh et al.*, 2012; *Kamp et al.*, 2013).

5.2.1. *General distribution of gaseous water*

Fig. 8 shows the distribution of water vapor in a typical kinetic chemical disk model with radius R and height z. The disk gas temperature distribution is crucial for the chemistry. It is commonly recognized that dust on the disk surface is warmer than in the midplane due to direct stellar photon heating (*Calvet et al.*, 1992; *Chiang and Goldreich*, 1997). Furthermore the gas temperature is decoupled from the dust in the upper layers due to direct gas heating (e.g., *Kamp and Dullemond*, 2004). There are roughly 3 areas where water vapor is predicted to be abundant and therefore possibly emissive (see also discussion in *Woitke et al.*, 2009a). These 3 areas or "regions" are labelled with coordinates (radial and vertical) that are specific to the physical structure (radiation field, temperature, density, dust properties) of this model. Different models (with similar dust- and gas-rich conditions) find the same general structure, but not at the exact same physical location.

Region 1 (R = inner radius to 1.5 AU; $z/R < 0.1$): this region coincides with the condensation/sublimation front in the midplane at the snow line. Inside the snow line water vapor will be abundant. Reaction timescales imposed by chemical kinetics limit the overall abundance depending on the gas temperature. As seen in Fig. 8, if the gas temperature exceeds ~ 400 K then the midplane water will be quite abundant, carrying all available oxygen not locked in CO and refractory grains. If the gas temperature is below this value, but above the sublimation temperature of ~ 160 K, then chemical kinetics could redistribute the oxygen towards other species. During the early gas- and dust-rich stages up to a few Myr, this water vapor dominated region will persist and is seen in nearly all models. However, as solids grow, the penetrating power of UV radiation is increased. Since water vapor is sensitive to photodissociation by far-UV, this could lead to gradual decay of this layer, which would be consistent with the non-detection of water vapor inside the gaps of a small sample of transition disks (e.g., *Pontoppidan et al.*, 2010a; *Zhang et al.*, 2013).

Region 2 ($R > 20$ AU; surface layers and outer disk midplane): In these disk layers the *dust* temperature is uniformly below the sublimation temperature of water. Furthermore at these high densities ($n > 10^6$ cm^{-3}) atoms and molecules freeze out on dust grains on short timescales (§2.4). Under these circumstances, in the absence of non-thermal desorption mechanisms, models predict strong freeze-out with the majority of available oxygen present on grains as water ice. Much of this may be primordial water ice supplied by the natal cloud (*Visser et al.*, 2011, Fig. 5).

The detection of rotationally cold water vapor emission in the outer disk of TW Hya demonstrates that a tenuous layer of water vapor is present and that some non-thermal desorption process is active (*Hogerheijde et al.*, 2011). The leading candidate is photodesorption of water ice (*Dominik et al.*, 2005; *Öberg et al.*, 2009), as discussed in § 2.4.4, particularly given the high UV luminosities of T Tauri stars (*Yang et al.*, 2012a). This UV excess is generated by accretion and dominated by Lyα line emission (*Schindhelm et al.*, 2012).

Once desorbed as OH and H_2O, the UV radiation then also destroys the water vapor molecules leading to a balance between these processes and a peak abundance near $(1-3) \times 10^{-7}$ (*Dominik et al.*, 2005; *Hollenbach et al.*, 2009). In general most models exhibit this layer, which is strongly dependent on the location and surface area of ice-coated grains (i.e. less surface area reduces the effectiveness of photodesorption). Direct comparison of models with observations finds that the amount of water vapor predicted to be present exceeds the observed emission (*Bergin et al.*, 2010; *Hogerheijde et al.*, 2011). This led to the suggestion that the process of grain growth and sedimentation could operate to remove water ice from the UV exposed disk surface layers. This is consistent with spectroscopic data of the TW Hya scattered light disk, which do not show water ice features in the spectrum originating from this layer (*Debes et al.*, 2013). However, further fine tuning of this settling mechanism is needed (*Dominik and Dullemond*, in prep., *Akimkin et al.*, 2013). An alternative explanation may be a smaller dust disk compared with the gas disk (*Qi et al.*, 2013).

Region 3 ($R < 20$ AU; $z/R > 0.1$): Closer to the exposed disk surface the gas and dust become thermally decoupled. The density where this occurs depends on the relative amount of dust grains in the upper atmosphere, which may be altered by dust coagulation and settling (*Jonkheid et al.*, 2004; *Nomura et al.*, 2007) and on the thermal accommodation of the dust gas interaction (*Burke and Hollenbach*, 1983). In these decoupled layers $T_{\rm gas} \gg T_{\rm dust}$, and when the gas temperature exceeds a few hundred K the neutral-neutral gas-phase pathways for water formation become efficient, leading to water abundances of order 10^{-5} (Fig. 8).

More directly, the disk surface is predicted to be water vapor rich at gas temperatures $\gtrsim$ few hundred K and dust temperatures $\sim$100 K. Indeed, there should exist surface layers at radii where the midplane temperature is sufficiently low to freeze water vapor, but where the surface can

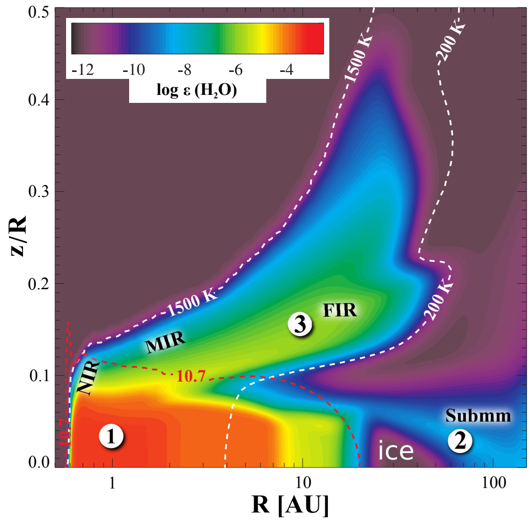

Fig. 8.— Abundance of gaseous water relative to total hydrogen as a function of radial distance, R, and relative height above the midplane, z/R, for a disk around an A-type star (T_*=8600 K). Three regions with high H_2O abundance can be distinguished. Regions 1 and 3 involve high-temperature chemistry, whereas region 2 lies beyond the snow line and involves photodesorption of water ice. The white contours indicate gas temperatures of 200 and 1500 K, whereas the red contour shows the $n_{\rm H} = 5 \times 10^{10}$ cm^{-3} density contour. From *Woitke et al.* (2009b).

support water formation via the high-temperature chemistry (i.e., region 3 goes out to larger radii than region 1). Thus the water zone on the disk surface presents the largest surface area and it is this water that is readily detected with current astronomical observations of high-lying transitions of $H_2^{16}O$ with *Spitzer* and *Herschel*. The snow line in the midplane is thus potentially hidden by the forest of water transitions produced by the hot chemistry on the surface.

There are some key dependences and differences which can be highlighted. One important factor is the shape of the UV radiation field. In general, models that use a scaled interstellar UV radiation field, for example based on FUSE/IUE/HST observations of the UV excess (*Yang et al.*, 2012a), neglect the fact that some molecules like H_2 and CO require very energetic photons to photodissociate, which are not provided by very cool stars. A better approach is to take the actual stellar continua into account (*van Dishoeck et al.*, 2006), with UV excess due to accretion added where appropriate (*van Zadelhoff et al.*, 2003). A very important factor in this regard is the relative strength of the Lyα line to the overall UV continuum. Observations find that Lyα has nearly an order of magnitude more UV flux than the stellar FUV continuum in accreting sources (*Bergin et al.*, 2003; *Schindhelm et al.*, 2012). In addition because of the difference in scattering (Lyα isotropic from H atom surface; UV continuum anisotropic from dust grains), Lyα will dominate the radiation field deeper into the disk (*Bethell and Bergin*, 2011).

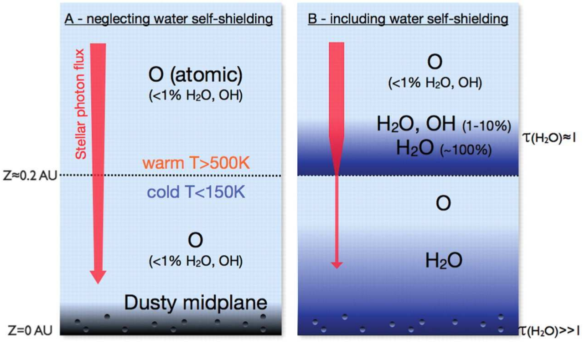

Fig. 9.— Cartoon illustrating the water self-shielding mechanism and the resulting vertical stratification of O and H_2O. Inclusion of water self-shielding in the upper layers leads to a 'wet' warm layer. From *Bethell and Bergin* (2009).

Most models find the presence of this warm water layer in dust-dominated disks. However, *Bethell and Bergin* (2009) suggest that water can form in such high abundances in the surface layer that it mediates the transport of the energetic UV radiation by becoming self-shielding (Fig. 9). If this is the case, then the surface water would survive for longer timescales, because it is somewhat decoupled from the dust evolution. As a consequence water and chemistry in the midplane might be protected even as the FUV absorbing dust grains settle to the midplane.

Additional factors of importance for the survival of this emissive surface layer are the gas temperature and molecular hydrogen abundance. Although theoretical solutions for the gas temperature are inherently uncertain, it is clear that hot ($T_{\rm gas}$ > few hundred K) layers exist on disk surfaces (*Bruderer et al.*, 2012). However, as the gas disk dissipates, the accretion rate onto the star decays on timescales of a few Myr. Thus the UV luminosity that is associated with this accretion declines and the disk will cool down, cutting off the production of water from the hot ($T \gtrsim 400$ K) gas-phase chemistry on the exposed surface. In addition, as shown by *Glassgold et al.* (2009) and *Ádámkovics et al.* (2013), the formation of surface water requires the presence of H_2 to power the initiating reaction. Finally, vertical mixing through turbulence or disk winds can bring water ice from the lower to the upper layers where the ice sublimates and adds to the oxygen budget and water emission (*Heinzeller et al.*, 2011).

5.2.2. *Planetesimal formation and water ice transport*

The dust particles in disks collide and grow, with water ice mantles generally thought to help the coagulation processes. The evolution of dust to pebbles, rocks and planetesimals (1–100 km bodies, the precursors of comets and asteroids) is described in the chapters by *Testi et al.* and *Johansen et al.*. The disk models cited above do not take into account transport of ice-rich planetesimals from the cold outer to the warm inner disk, even though such radial drift is known to be highly effective at a few AU for rocks up to meter size (or mm size further out in the disk) (e.g., *Weidenschilling and Cuzzi*, 1993). This drift of icy planetesimals can be a source of water vapor enrichment inside the snow line (*Ciesla and Cuzzi*, 2006). The astrophysical signature of this phenomenon would be the presence of water vapor in the inner disk with an abundance greater than the stellar oxygen abundance, because the planetesimals are hydrogen-poor, that is, the main volatile species, H_2, is not present in water-rich planetesimal ices. Some of this hot water can diffuse outwards again and re-condense just outside the snowline (the cold finger effect. Fig. 7) which increases the density of solids by a factor of 2–4 and thereby assists planet formation (*Stevenson and Lunine*, 1988). Alternatively, icy grains can be trapped in pressure bumps where they can grow rapidly to planetesimals before moving inward (e.g., *van der Marel et al.*, 2013).

6. WATER IN THE OUTER SOLAR SYSTEM

In the standard model of the disk out of which our solar system formed, the snow line was at 2.7 AU at the end of the gas-rich phase (*Hayashi*, 1981). This snow line likely moved inward from larger distances in the early embedded phase (*Kennedy and Kenyon*, 2008). Thus, it is no surprise that water ice is a major constituent of all solar system bodies that formed and stayed beyond the snow line. Nevertheless, their water ice content, as measured by the mass in ice with respect to total ice+rock mass can differ substantially, from <1% for some asteroids to typically 50% for comets. Also, the observational signatures of water on these icy bodies and its isotopic ratio can differ. In the following sections, we review our knowledge of water ice in the present-day solar system. In § 8, possible mechanisms of supplying water from these reservoirs to the terrestrial planet zone will be discussed.

6.1. Outer asteroid belt

Since the outer asteroid belt is located outside the Hayashi snow line, it provides a natural reservoir of icy bodies in the solar system. This part of the belt is dominated by so-called C, P and D class asteroids with sizes up to a few 100 km at distances of $\sim$3, 4 and $\geq$4 AU, respectivily, characterized by their particularly red colors and very low albedos, $\lesssim 0.1$ (*Bus and Binzel*, 2002). Because of their spectroscopic similarities to the chemically primitive carbonaceous chondrites found as meteorites on Earth, C-type asteroids have been regarded as largely unaltered, volatile-rich bodies. The P- and D-types may be even richer in organics.

The water content in these objects has been studied though IR spectroscopy of the 3 μm band. In today's solar system, any water ice on the surface would rapidly sublimate at the distance of the belt, so only water bonded to the rocky silicate surface is expected to be detected. Hydrated minerals can be formed if the material has been in contact with liquid water. The majority of the C-type asteroids show hydrated silicate absorption, indicating that they indeed underwent heating and aqueous alteration episodes (*Jones et al.*, 1990, and refs. therein). However, only 10% of the P and D-type spectra show weak water absorption, suggesting that they have largely escaped this processing and that the abundance of hydrated silicates gradually declines in the outer asteroid belt. Nevertheless, asteroids that do not display water absorption on their surfaces (mostly located beyond 3.5 AU) may still retain ices in their interior. Indeed, water fractions of 5–10% of their total mass have been estimated. This is consistent with models that show that buried ice can persist in the asteroid belt within the top few meters of the surface over billions of years, as long as the mean surface temperature is less than about 145 K (*Schorghofer*, 2008). Water vapor has recently been detected around the dwarf planet Ceres at 2.7 AU in the asteroid belt, with a production rate of at least 10^{26} mol s^{-1}, directly confirming the presence of water (*Küppers et al.*, 2014).

Hsieh and Jewitt (2006) discovered a new population of small objects in the main asteroid belt, displaying cometary characteristics. These so-called main belt comets (ten are currently known) display clearly asteroidal orbits, yet have been observed to eject dust and thus satisfy the observational definition of a comet. These objects are unlikely to have originated elsewhere in the solar system and to have subsequently been trapped in their current orbits. Instead, they are intrinsically icy bodies, formed and stored at their current locations, with their cometary activity triggered by some recent event.

Since main belt comets are optically faint, it is not known whether they display hydration spectral features that could point to the presence of water. Activity of main belt comets is limited to the release of dust and direct outgassing of volatiles, like for Ceres, has so far not been detected. The most stringent indirect upper limit for the water production rate derived from CN observations is that in the prototypical main belt comet 133P/Elst-Pizarro $< 1.3 \times 10^{24}$ mol s^{-1} (*Licandro et al.*, 2011), which is subject to uncertainties in the assumed water-to-CN abundance ratio. For comparison, this is five orders of magnitude lower than the water production rate of comet Hale-Bopp. Its mean density is 1.3 gr cm^{-3} suggesting a moderately high ice fraction (*Hsieh et al.*, 2004). *Herschel* provided the most stringent direct upper limits for water outgassing in 176P/LINEAR ($< 4 \times 10^{25}$ mol s^{-1}, 3σ; *de Val-Borro et al.* 2012) and P/2012 T1 PANSTARRS ($< 8 \times 10^{25}$ mol s^{-1}; *O'Rourke et al.* 2013).

Another exciting discovery is the direct spectroscopic detection of water ice on the asteroid 24 Themis (*Campins et al.*, 2010; *Rivkin and Emery*, 2010), the largest (198 km diameter) member of the Themis dynamical family at $\sim$3.2 AU, which also includes three main belt comets. The 3.1 μm spectral feature detected in Themis is significantly different from those in other asteroids, meteorites and all plausible mineral samples available. *Campins et al.* (2010) argue that the observations can be accurately matched by small ice particles evenly distributed on the surface. A subsurface ice reservoir could also be present if Themis underwent differentiation resulting in a rocky core and an ice mantle. *Jewitt and Guilbert-Lepoutre* (2012) find no direct evidence of outgassing from the surface of Themis or Cybele with a 5σ upper limit for the water production rate 1.3×10^{28} mol s^{-1}, assuming a cometary water-to-CN mixing ratio. They conclude that any ice that exists on these bodies should be relatively clean and confined to a $<$10% fraction of the Earth-facing surface.

Altogether, these results suggest that water ice may be common below asteroidal surfaces and widespread in asteroidal interiors down to smaller heliocentric distances than previously expected. Their water contents are clearly much higher than those of meteorites that originate from the inner asteroid belt, which have only 0.01% of their mass in water (*Hutson and Ruzicka*, 2000).

6.2. Comets

Comets are small solar system bodies with radii less than 20 km that have formed and remained for most of their lifetimes at large heliocentric distances. Therefore, they likely contain some of the least-processed, pristine ices from the solar nebula disk. They have often been described as 'dirty snowballs', following the model of *Whipple* (1950), in which the nucleus is visualized as a conglomerate of ices, such as water, ammonia, methane, carbon dioxide, and carbon monoxide, combined with meteoritic materials. However, *Rosetta* observations during the Deep Impact encounter (*Küppers et al.*, 2005) suggest a dust-to-gas ratio in excess of unity in comet 9P/Tempel 1. Typically, cometary ice/rock ratios are of order unity with an implied porosity well over 50% (*A'Hearn*, 2011).

The presence and amount of water in comets is usually quantified through their water production rates, which are traditionally inferred from radio observations of its photodissociation product, OH, at 18 cm (*Crovisier et al.*, 2002). Measured rates vary from 10^{26} to 10^{29} mol s^{-1}. The first direct detection of gaseous water in comet 1P/Halley, through its ν_3 vibrational band at 2.65 μm, was obtained using the KAO (*Mumma et al.*, 1986). The 557 GHz transition of ortho-water was observed by *SWAS* (*Neufeld et al.*, 2000) and *Odin* (*Lecacheux et al.*, 2003), whereas *Herschel* provided for the first time access to multiple rotational transitions of both ortho- and para-water (*Hartogh et al.*, 2011). These multi-transition mapping observations show that the derived water production rates are sensitive to the details of the excitation model used, in particular the ill-constrained temperature profile within the coma, with uncertainties up to 50% (*Bockelée-Morvan et al.*, 2012).

Dynamically, comets can be separated into two general groups: short-period, Jupiter-family comets and long-period comets (but see *Horner et al.* 2003 for a more detailed classification). Short-period comets are thought to originate from the Kuiper belt, or the associated scattered disk, beyond the orbit of Neptune, while long-period comets formed in the Jupiter-Neptune region and were subsequently ejected into the Oort cloud by gravitational interactions with the giant planets. In reality, the picture is significantly more complex due to migration of the giant planets in the early solar system (see below). In addition, recent simulations (*Levison et al.*, 2010) suggest that the Sun may have captured comets from other stars in its birth cluster. In this case, a substantial fraction of the Oort-cloud comets, perhaps in excess of 90%, may not even have formed in the Sun's protoplanetary disk. Consequently, there is increasing emphasis on classifying comets based on their chemical and isotopic composition rather than orbital dynamics (*Mumma and Charnley*, 2011). There is even evidence for heterogeneity within a single comet, illustrating that comets may be built up from cometesimals originating at different locations in the disk (*A'Hearn*, 2011).

Traditionally, the ortho-to-para ratio in water and other cometary volatiles has been used to contrain the formation and thermal history of the ices. Recent laboratory experiments suggest that this ratio is modified by the desorption processes, both thermal sublimation and photodesorption, and may therefore tell astronomers less about the water formation location than previously thought (see discussions in *van Dishoeck et al.* 2013 and *Tielens* 2013).

6.3. Water in the outer satellites

Water is a significant or major component of almost all moons of the giant planets for which densities or spectral information are available. Jupiter's Galilean moons exhibit a strong gradient from the innermost (Io, essentially all rock, no ice detected) to the outermost (Callisto, an equal mixture of rock and ice). Ganymede has nearly the same composition and hence rock-to-ice ratio as Callisto. Assuming that the outermost of the moons reflects the coldest part of the circumplanetary disk out of which the moons formed, and hence full condensation of water, Callisto's (uncompressed) density matches that of solar-composition material in which the dominant carbon-carrier was methane rather than carbon monoxide (*Wong et al.*, 2008). The fact that Callisto has close to (but not quite) the full complement of water expected based on the solar oxygen abundance implies that the disk around Jupiter had a different chemical composition (CH_4-rich, CO-poor) from that of the solar nebula disk, which was CO-dominated (*Prinn and Fegley*, 1981).

The Saturnian satellites are very different. For satellites large enough to be unaffected by porosity, but excluding massive Titan, the ice-to-rock ratio is higher than for the Galilean moons (*Johnson and Estrada*, 2009). However, Titan—by far the most massive moon—has a bulk density and mass just in between, and closely resembling, Ganymede's and Callisto's. Evidently the Saturnian satellite system had a complex collisional history, in which the original ice-rock ratio of the system was not preserved except perhaps in Titan. The moon Enceladus, which exhibits volcanic and geyser activity, offers the unique opportunity to sample Saturnian system water directly. Neptune's Triton, like Pluto, has a bulk density and hence ice-rock ratio consistent with what is expected for a solar nebula disk in which CO dominated over CH_4. Its water fraction is about 15–35%. At this large distance from the Sun, N_2 can also be frozen out and Triton's spectrum is indeed dominated by N_2 ice with traces of CH_4 and CO ices; the water signatures are much weaker than on other satellites (*Cruikshank et al.*, 2000). The smaller Trans Neptunion Objects (TNOs) ($<$few hundred km size) are usually found to have mean densities around 1 g cm^{-3} and thus a high ice fraction. Larger TNOs such as Quaoar and Haumea have much higher densities (2.6–3.3 g cm^{-3}) suggesting a much lower ice content, even compared with Pluto (2.0 g cm^{-3}) (*Fornasier et al.*, 2013).

In summary, the water ice content of the outer satellites varies with position and temperature, not only as a function of distance from the Sun, but also from its parent planet. Ice fractions are generally high ($\geq$50%) in the colder parts and consistent with solar abundances depending on the amount of oxygen locked up in CO. However, collisions can have caused a strong reduction of the water ice content.

6.4. Water in the giant planets

The largest reservoirs of what was once water ice in the solar nebula disk are presumably locked up in the giant planets. If the formation of giant planets started with an initial solid core of 10–15 Earth masses with subsequent growth from a swarm of planetesimals of ice and rock with solar composition, the giant planets could have had several Earth masses of oxygen, some or much of which may have been in water molecules in the original protoplanetary disk. The core also gravitationally attracts the surrounding gas in the disk consisting mostly of H and He with the other elements in solar composition. The resulting gas giant planet has a large mass and diameter, but a low overall density compared with rocky planets. The giant planet atmosphere is expected to have an excess in heavy elements, either due to the vaporization of the icy planetesimals when they entered the envelopes of the growing planet during the heating phase, or due to partial erosion of the original core, or both (*Encrenaz*, 2008; *Mousis et al.*, 2009). These calculations assume that all heavy elements are equally trapped within the ices initially, which is a debatable assumption, and that the ices fully evaporate, with most of the refractory material sedimenting onto the core. In principle, the excesses provide insight into giant planet formation mechanisms and constraints on the composition of their building blocks.

6.4.1. Jupiter and Saturn

For Jupiter, elemental abundances can be derived from spectroscopic observations and from data collected by the Galileo probe, which descended into the Jovian atmosphere. Elements like C, N, S and the noble gases Ar, Kr and Xe, have measured excesses as expected at 4$\pm$2 (*Owen and Encrenaz*, 2006). However, O appears to show significant depletion. Unfortunately, the deep oxygen abundance in

Jupiter is not known. The measured abundance of gaseous water—the primary carrier of oxygen in the Jovian atmosphere since there is little CO—provides only a lower limit since the troposphere at about 100 mbar is a region of minimum temperature ($\sim$110 K for Jupiter) and therefore acts as a cold trap where water can freeze out. Thus, the amount of gaseous water is strongly affected by condensation and rainout associated with large-scale advective motions (*Showman and Dowling*, 2000), meteorological processes (*Lunine and Hunten*, 1987), or both. The Galileo probe fell into a so-called 'hot spot' (for the excess brightness observed in such regions at 5 μm wavelengths), with enhanced transparency and hence depleted in water, and is thus not representative of the planet as a whole. The water abundance, less than 1/10 the solar value in the upper atmosphere, was observed to be higher at higher pressures, toward the end of the descent (*Roos-Serote et al.*, 2004). The sparseness of the measurements made it impossible to know whether the water had 'leveled out' at a value corresponding to 1/3 solar or would have increased further had the probe returned data below the final 21 bar level.

As noted above, predictions for standard models of planetesimal accretion—where volatiles are either adsorbed on, or enclathrated in, water ice—give oxygen abundances 3–10 times solar in the Jovian deep interior. Although atmospheric explanations for the depleted water abundance in Jupiter are attractive, one must not rule out the possibility that water truly is depleted in the Jovian interior—that is, the oxygen-to-hydrogen ratio in Jupiter is less enriched than the carbon value at 4$\pm$2 times solar. A motivation for making such a case is that at least one planet with a C/O$>$1—a 'carbon-rich planet'—has been discovered (*Madhusudhan et al.*, 2011a), companion to the star WASP12a with a C/O ratio of 0.44, roughly solar. One explanation is that the portion of this system's protoplanetary disk was somehow depleted in water at the time the planet formed and acquired its heavy element inventory (*Madhusudhan et al.*, 2011b).

Prior to this discovery, the possibility of a carbon-rich Jupiter was considered on the basis of the Galileo results alone by *Lodders* (2004) who proposed that in the early solar system formation the snow line might have been further from the Sun than the point at which Jupiter formed, and volatiles adhering to solid organics rather than water ice were carried into Jupiter.

Mousis et al. (2012) looked at the possibility that Jupiter may have acquired planetesimals from an oxygen-depleted region by examining element-by-element the fit to the Galileo probe data of two contrasting models: one in which the planetesimal building blocks of Jupiter derived from a disk with C/O= 1/2 (roughly, the solar value), and the other in which C/O=1. Within the curent error bars, the two cases cannot be distinguished. However, any determination of the deep oxygen abundance in Jupiter yielding an enrichment of less than 2 times solar would be a strong argument in favor of a water depletion, and thus high C/O ratio, at certain places and times in the solar nebula disk.

Are such depletions plausible? A wide range of oxidation states existed in the solar nebula disk at different times and locations. For example, the driest rocks, the enstatite chondrites, are thought to have come from parent bodies formed inward of all the other parent bodies, and their mineralogy suggests reducing conditions—consistent with a depleted water vapor abundance—in the region of the nebula where they formed (*Krot et al.*, 2000). One recent model of the early evolution of Jupiter and Saturn hypothesizes that these giant planets moved inward significantly during the late stages of their formation, reaching 1.5 AU in the case of Jupiter (*Walsh et al.*, 2011), almost certainly inward of the snow line (see § 8.2). If planetesimals in this region accreted volatiles on refractory organic and silicate surfaces which were then incorporated into Jupiter, the latter would appear carbon-rich and oxygen-depleted. However, temperatures in that region may not have been low enough to provide sufficient amounts of the more volatile phases. A second possibility is that Jupiter's migration scattered these water poor planetesimals to the colder outer solar system, where they trapped noble gases and carbon-and nitrogen-bearing species at lower temperature—but water ice, already frozen out, was not available.

In order to test such models, one must directly determine the abundance of oxygen-bearing species in Jupiter and if possible, in Saturn. The case of Saturn is similar to that of Jupiter in the sense that the carbon excess as derived from CH_4 spectroscopy is as expected, but again no reliable oxygen abundance can be determined. Under the conditions present in the Jovian envelope at least (if not its core), water will dominate regardless of the initial carbon oxidation state in the solar nebula. NASA's *Juno* mission to Jupiter will measure the water abundance down to many tens of bars via a microwave radiometer (MWR) (*Janssen et al.*, 2005). Complementary to the MWR is a near-infrared spectrometer JIRAM (Jovian Infrared Auroral Mapper), that will obtain the water abundance in the meteorological layer (*Adriani et al.*, 2008). The two instruments together will be able to provide a definitive answer for whether the water abundance is below or above solar, and in the latter case, by how much, when *Juno* arrives in 2016. *Juno* will also determine the mass of the heavy element core of Jupiter, allowing for an interpretation of the significance of the envelope water abundance in terms of total oxygen inventory.

There is no approved mission yet to send a probe into Saturn akin to Galileo. However, the *Cassini* Saturn Orbiter will make very close flybys of Saturn starting in 2016, similar to what *Juno* will do at Jupiter. Unfortunately, a microwave radiometer akin to that on *Juno* is not present on *Cassini*, but a determination of the heavy element core mass of Saturn may be obtained from remote sensing. In summary, the fascinating possibility that Jupiter and Saturn may have distinct oxygen abundances because they sampled at different times and to differing extents regions of the solar nebula disk heterogeneous in oxygen (i.e., water) abundance is testable if the bulk oxygen abundances can be measured.

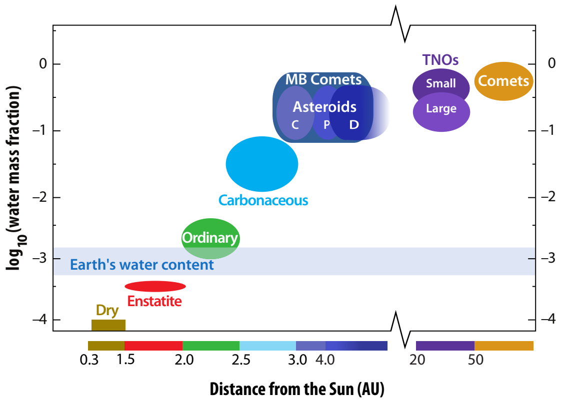

Fig. 10.— Water content of various parent bodies at the time of Earth's growth as a function of radial distance from the Sun. Enstatite chondrites originating from asteroids around 1.8 AU in the inner disk are very dry. In contrast, carbonaceous chondrites originating from the outer asteroid belt and beyond have a water content of 5–10%, and main belt comets, TNOs and regular comets even more. Figure by M. Persson, adapted from *Morbidelli et al.* (2012).

6.4.2. *Uranus and Neptune*

The carbon excesses measured from CH_4 near-infrared spectroscopy give values of 30–50 for Uranus and Neptune, compared with 9 and 4 for Saturn and Jupiter (*Encrenaz*, 2008). These values are consistent with the assumption of an initial core of 10–15 Earth masses with heavy elements in solar abundances. Unfortunately, nothing is known about the water or oxygen content in Uranus and Neptune, since water condensation occurs at such deep levels that even tropospheric water vapor cannot be detected. Unexpectedly, ISO detected water vapor in the upper atmospheres of both ice giants, with mixing ratios orders of magnitude higher than the saturation level at the temperature inversion (*Feuchtgruber et al.*, 1997). These observations can only be accounted for by an external flux of water molecules, due to interplanetary dust, or sputtering from rings or satellites. Similarly, *Herschel* maps of water of Jupiter demonstrate that even 15 years after the Shoemaker-Levy 9 impact, more than 95% of the stratospheric Jovian water comes from the impact (*Cavalié et al.*, 2013). On the other hand, the low D/H ratios in molecular hydrogen measured by *Herschel* in the atmospheres of Uranus and Neptune may imply a lower ice mass fraction of their cores than previously thought (14–32%) (*Feuchtgruber et al.*, 2013) .

It is unlikely that information on the deep oxygen abundance will be available for Uranus and Neptune anytime soon, since reaching below the upper layers to determine the bulk water abundance is very difficult. Thus, data complementary to that for Jupiter and Saturn will likely come first from observations of Neptune-like exoplanets.

7. WATER IN THE INNER SOLAR SYSTEM

Terrestrial planets were formed by accretion of rocky planetesimals, and they have atmospheres that are only a small fraction of their total masses. They are small and have high densities compared with giant planets. Earth and Venus have very similar sizes and masses, whereas Mars has a mass of only 10% of that of Earth and a somewhat lower density (3.9 vs 5.2 gr cm^{-3}). Terrestrial planets undergo different evolutionary processes compared with their gas-rich counterparts. In particular, their atmospheres result mostly from outgassing and from external bombardment. Internal differentiation of the solid material after formation leads to a structure in which the heavier elements sink to the center, resulting in a molten core (consisting of metals like iron and nickel), a mantle (consisting of a viscous hot dense layer of magnesium rich silicates) and a thin upper crust (consisting of colder rocks).

Water has very different appearances on Venus, Earth and Mars, which is directly related to their distances from the Sun at 0.7, 1.0 and 1.7 AU, respectively. On Venus, with surface temperatures around 730 K, only gaseous water is found, whereas the surface of Mars has seasonal variations ranging from 150–300 K resulting in water freezing and sublimation. Its current mean surface pressure of 6 mbar is too low for liquid water to exist, but there is ample evidence for liquid water on Mars in its early history. Most of the water currently on Mars is likely subsurface in the crust down to 2 km depth. Earth is unique in that its mean surface temperature of 288 K and pressure of 1 bar allow all three forms of water to be present: vapor, liquid and ice. In § 8, the origin of water on these three planets will be further discussed. It is important to keep in mind that even though these planets have very different atmospheres today, they may well have started out with comparable initial water mass fractions and similar atmospheric compositions dominated by H_2O, CO_2, and N_2 (*Encrenaz*, 2008).

Earth has a current water content that is non-negligible. The mass of the water contained in the Earth's crust (including the oceans and the atmosphere) is 2.8×10^{-4} Earth masses, denoted as 'one Earth ocean' because almost all of this is in the surface waters of the Earth. The mass of the water in the present-day mantle is uncertain. *Lécuyer et al.* (1998) estimate it to be in the range of $(0.8\text{–}8)\times10^{-4}$ Earth masses, equivalent to 0.3–3 Earth oceans. More recently, *Marty* (2012) provides arguments in favor of a mantle water content as high as $\sim$7 Earth oceans. However, an even larger quantity of water may have resided in the primitive Earth and been subsequently lost during differentiation and impacts. Thus, the current Earth has a water content of roughly 0.1% by mass, larger than that of enstatite chondrites, and it is possible that the primitive Earth had a water content comparable with or larger than that of ordinary chondrites, definitely larger than the water content of meteorites and material that condensed at 1 AU (Fig. 10).

Remote sensing and space probes have detected water in the lower atmosphere of Venus at a level of a few tens of parts per millions (*Gurwell et al.*, 2007), confirming that it is a minor component. Radar images show that the surface of Venus is covered with volcanoes and is likely very young, only 1 billion years. Direct sampling of the Venusian crust is needed to determine the extent of past and present hydration which will provide an indication of whether Venus once had an amount of water comparable to that on Earth. Hints that there may have been much more water on Venus and Mars come from D/H measurements (see § 8.1).

8. ORIGIN OF WATER TERRESTRIAL PLANETS

Earth, Mars and perhaps also Venus all have water mass fractions that are higher than those found in meteorites in the inner solar nebula disk. Where did this water come from, if the local planetesimals were dry? There are two lines of arguments that provide clues to its origin. One clue comes from measuring the D/H ratio of the various water mass reservoirs. The second argument looks at the water mass fractions of various types of asteroids and comets, combined with the mass delivery rates of these objects on the young planets at the time of their formation, based on models of the dynamics of these planetesimals. For example, comets have plenty of water, but the number of comets that enter the inner 2 AU and collide with proto-Earth or -Mars is small. To get one Earth ocean, $\sim 10^8$ impacting comets are needed. It is therefore not a priori obvious which of the reservoirs shown in Fig. 10 dominates.

Related to this point is the question whether the planets formed 'wet' or 'dry'. In the wet scenario, the planets either accreted a water-rich atmosphere or they formed from planetesimals with water bonded to silicate grains at 1 AU, with subsequent outgassing of water as the material is heated up during planet formation. In the dry scenario, the terrestrial planets are initially built up from planetesimals with low water mass fractions and water is delivered to their surfaces by water-rich planetesimals, either late in the building phase, or even later after the planets have formed and differentiated. If after differentiation, this scenario is often called a 'late veneer'. In the following, we first discuss the D/H ratios and then come back to the mass fraction arguments.

8.1. D/H ratios in solar system water reservoirs

The D/H ratio of water potentially provides a unique fingerprint of the origin and thermal history of water. Figure 11 summarizes the various measurements of solar system bodies, as well as interstellar ices and protostellar objects.

The primordial [D]/[H] ratio set shortly after the Big Bang is 2.7×10^{-5}. Since then, deuterium has been lost due to nuclear fusion in stars, so the deuterium abundance at the time of our solar system formation, 4.6 billion years ago (redshift of about $z \approx 1.4$), should be lower than the primordial value, but higher than the current day interstellar [D]/[H] ratio. The latter value has been measured in the diffuse local interstellar medium from UV absorption lines of atomic D and H, and varies from place to place but can be as

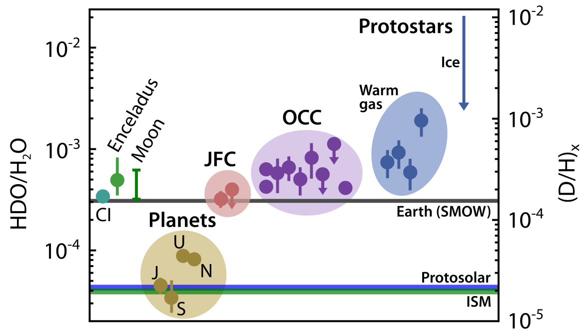

Fig. 11.— D/H ratio in water in comets and warm protostellar envelopes compared to values in the Earth oceans, the giant planets, the solar nebula disk, and the interstellar medium. Values for carbonaceous meteorites (CI), the Moon and Saturn's moon Enceladus are presented as well. Note that both $(D/H)_X$, the deuterium to hydrogen ratio in molecule X, and HDO/H_2O are plotted; measured HD/H_2 and HDO/H_2O ratios are $2\times(D/H)_X$. Figure by M. Persson, based on *Bockelée-Morvan et al.* (2012) and subsequent measurements cited in the text. The protostellar data refer to warm gas (*Persson et al.*, 2013, and subm.)

high as 2.3×10^{-5} (*Prodanović et al.*, 2010). These higher values suggest that relatively little deuterium has been converted in stars, so a [D]/[H] value of the solar nebula disk only slightly above the current ISM value is expected at the time of solar system formation. The solar nebula [D]/[H] ratio can be measured from the solar wind composition as well as from HD/H_2 in the atmospheres of Jupiter and Saturn and is found to be $(2.5 \pm 0.5) \times 10^{-5}$ (*Robert et al.*, 2000, and references cited), indeed in-between the primordial and the current ISM ratios.[4]

The D/H ratio of Earth's ocean water is 1.5576×10^{-4} ('Vienna Standard Mean Ocean Water', VSMOW or SMOW). Whether this value is representative of the bulk of Earth's water remains unclear, as no measurements exist for the mantle or the core. It is thought that recycling of water in the deep mantle does not significantly change the D/H ratio. In any case, the water D/H ratio is at least a factor of 6 higher than that of the gas out of which our solar system formed. Thus, Earth's water must have undergone fractionation processes that enhance deuterium relative to hydrogen at some stages during its history, of the kind described in § 2.4 for interstellar chemistry at low temperatures.

Which solar system bodies show D/H ratios in water similar to those found in Earth's oceans? The highest [D]/[H] ratios are found in two types of primitive meteorites (*Robert et al.*, 2000): LL3, an ordinary chondrite that may have the near-Earth asteroid 433 Eros as its parent body (up to a factor of 44 enhancement compared to the protosolar ratio in H_2) and some carbonaceous chondrites (a factor of 15 to 25 enhancement). Most chondrites show lower enhance-

[4]Note that measured HD/H_2 and HDO/H_2O ratios are $2\times(D/H)_X$, the D/H ratios in these molecules.

ments than the most primitive meteorites. Pre-*Herschel* observations of six Oort-cloud or long-period comets give a D/H ratio in water of $\sim 3 \times 10^{-4}$, a factor of 12 higher than the protosolar ratio in H_2 (*Mumma and Charnley*, 2011).

Herschel provided the first measurement of the D/H ratio in a Jupiter-family comet. A low value of $(1.61 \pm 0.24) \times 10^{-4}$, consistent with VSMOW, was measured in comet 103P/Hartley 2 (*Hartogh et al.*, 2011). In additon, a relatively low ratio of $(2.06 \pm 0.22) \times 10^{-4}$ was found in the Oort-cloud comet C/2009 P1 Garradd (*Bockelée-Morvan et al.*, 2012) and a sensitive upper limit of $< 2 \times 10^{-4}$ (3σ) was obtained in another Jupiter-family comet 45P/Honda-Mrkos-Pajdušáková (Lis et al. 2013). The Jupiter-family comets 103P and 45P are thought to originate from the large reservoir of water-rich material in the Kuiper belt or scattered disk at 30–50 AU. In contrast, Oort cloud comets, currently at much larger distances from the Sun, may have formed closer in, near the current orbits of the giant planets at 5–20 AU, although this traditional view has been challened in recent years (see § 6.2). Another caveat is that isotopic ratios in cometary water may have been altered by the outgassing process (*Brown et al.*, 2011). Either way, the *Herschel* observations demonstrate that the earlier high D/H values are not representative of all comets.

How do these solar system values compare with interstellar and protostellar D/H ratios? Measured D/H ratios in water in protostellar envelopes vary strongly. In the cold outer envelope, D/H values for gas-phase water are as high as 10^{-2} (*Liu et al.*, 2011; *Coutens et al.*, 2012, 2013), larger than the upper limits in ices of $<(2–5)\times10^{-3}$ obtained from infrared spectroscopy (*Dartois et al.*, 2003; *Parise et al.*, 2003). In the inner warm envelope, previous discrepancies for gaseous water appear to have been resolved in favor of the lower values, down to $(3–5)\times10^{-4}$ (*Jørgensen and van Dishoeck*, 2010a; *Visser et al.*, 2013; *Persson et al.*, 2013, and subm.) The latter values are within a factor of two of the cometary values.

Based on these data, the jury is still out whether the D/H ratio in solar system water was already set by ices in the early (pre-)collapse phase and transported largely unaltered to the comet-forming zone (cf. Fig. 4), or whether further alteration of D/H took place in the solar nebula disk along the lines described in § 2.4.5 (see also chapter by *Ceccarelli et al.*). The original D/H ratio in ices may even have been reset early in the embedded phase by thermal cycling of material due to accretion events onto the star (see chapter by *Audard et al.*). Is the high value of 10^{-2} found in cold gas preserved in the material entering the disk or are the lower values of $< 10^{-3}$ found in hot cores and ices more representative? Or do the different values reflect different D/H ratios in layered ices (*Taquet et al.*, 2013)?

Regardless of the precise initial value, models have shown that vertical and radial mixing within the solar nebula disk reduces the D/H ratios from initial values as high as 10^{-2} to values as low as 10^{-4} in the comet-forming zones (*Willacy and Woods*, 2009; *Yang et al.*, 2012b; *Jacquet and Robert*, 2013; *Furuya et al.*, 2013; *Albertsson et al.*, 2014). For water on Earth, the fact that the D enrichment is a factor $\sim$6 above the solar nebula value rules out the warm thermal exchange reaction of H_2O + HD $\rightarrow$ HDO + H_2 in the inner nebula ($\sim$1 AU) as the sole cause. Mixing with some cold reservoir with enhanced D/H at larger distances is needed.

Figure 11 contains values for several other solar system targets. Enceladus, one of Saturn's moons with volcanic activity, has a high D/H ratio consistent with it being built up from outer solar system planetesimals. Some measurements indicate that lunar water may have a factor of two higher hydrogen isotopic ratio than the Earth's oceans (*Greenwood et al.*, 2011), although this has been refuted (*Saal et al.*, 2013).

Mars and Venus have interestingly high D/H ratios. The D/H ratio of water measured in the Martian atmosphere is 5.5 times VSMOW, which is interpreted to imply a significant loss of water over Martian history and associated enhancement of deuterated water. Because D is heavier than H, it escapes more slowly, therefore over time the atmosphere is enriched in deuterated species like HDO. A time-dependent model for the enrichment of deuterium on Mars assuming a rough outgassing efficiency of 50% suggests that the amount of water that Mars must have accreted is 0.04–0.4 oceans. The amount of outgassing may be tested by Curiosity Mars rover measurements of other isotopic ratios, such as ^{38}Ar to ^{36}Ar.

The extremely high D/H ratio for water measured in the atmosphere of Venus, about 100 times VSMOW, is almost certainly a result of early loss of substantial amounts of crustal waters, regardless of whether the starting value was equal to VSMOW or twice that value. The amount of water lost is very uncertain because the mechanism and rate of loss affects the deuterium fractionation (*Donahue and Hodges*, 1992). Solar wind stripping, hydrodynamic escape, and thermal (Jeans') escape have very different efficiencies for the enrichment of deuterium per unit amount of water lost. Values ranging from as little as 0.1% to one Earth ocean have been proposed.

8.2. Water delivery to the terrestrial planet zone

8.2.1. Dry scenario

The above summary indicates at least two reservoirs of water ice rich material in the present-day solar system with D/H ratios consistent with that in Earth's oceans: the outer asteroid belt and the Kuiper belt or scattered disk (as traced by comets 103P and 45P). As illustrated in Fig. 10, these same reservoirs also have a high enough water mass fraction to deliver the overall water content of terrestrial planets. The key question is then whether the delivery of water from these reservoirs is consistent with the current understanding of the early solar system dynamics.

Over the last decade, there has been increasing evidence that the giant planets did not form and stay at their current location in the solar system but migrated through the protosolar disk. The Grand Tack scenario (*Walsh et al.*, 2011) invokes movement of Jupiter just after it formed in the early,

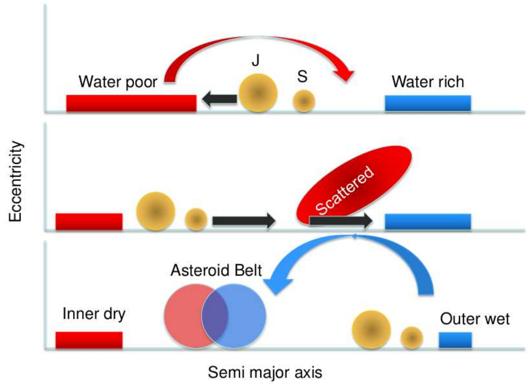

Fig. 12.— Cartoon of the delivery of water-rich planetesimals in the outer asteroid belt and terrestrial planet-forming zone based on the Grand Tack scenario in which Jupiter and Saturn first move inwards to 1.5 AU and then back out again. Figure based on *Walsh et al.* (2011).

gas-rich stage of the disk (few Myr). The Nice model describes the dynamics and migration of the giant planets in the much later, gas-poor phase of the disk, some 800–900 Myr after formation (*Gomes et al.*, 2005; *Morbidelli et al.*, 2005; *Tsiganis et al.*, 2005), see chapter by *Raymond et al.*

The Grand Tack model posits that if Jupiter formed earlier than Saturn just outside the snow line, both planets would have first migrated inward until they got locked in the 3:2 resonance, then they would have migrated outward together until the complete disappearance of the gas disk (see cartoon in Fig. 12). As summarized by *Morbidelli et al.* (2012), the reversal of Jupiter's migration at 1.5 AU provides a natural explanation for the outer edge of the inner disk of (dry) embryos and planetesimals at 1 AU, which is required to explain the low mass of Mars. The asteroid belt at 2–4 AU is first fully depleted and then repopulated by a small fraction of the planetesimals scattered by the giant planets during their formation. The outer part of this belt around 4 AU would have been mainly populated by planetesimals originally beyond the orbits of the giant planets (>5 AU), which explains similarities between primitive asteroids (C-type) and comets. Simulations by *Walsh et al.* (2011) show that as the outer asteroid belt is repopulated, $(3-11)\times10^{-2}$ Earth masses of C-type material enters the terrestrial planet region, which exceeds by a factor 6–22 the minimum mass required to bring the current amount of water to the Earth. In this picture, Kuiper belt objects would at best be only minor contributors to the Earth's water budget.

The Nice model identifies Jupiter and Saturn crossing their 1:2 orbital resonance as the next key event in the dynamical evolution of the disk in the gas-poor phase. After the resonance crossing time at $\sim$ 880 Myr, the orbits of the ice giants, Uranus and Neptune, became unstable. They then disrupted the outer disk and scattered objects throughout the solar system, including into the terrestrial planet region. However, *Gomes et al.* (2005) estimate the amount of cometary material delivered to the Earth to be only about 6% of the current ocean mass. A larger influx of material from the asteroid belt is expected, as resonances between the orbits of asteroids and giant planets can drive objects onto orbits with eccentricities and inclinations large enough to allow them to evolve into the inner solar system. By this time, the terrestrial planets should have formed already, so this material would be part of a 'late delivery'.

The Grand Tack model provides an attractive, although not unchallenged, explanation for the observed morphology of the inner solar system and the delivery of water to the Earth. In the asteroidal scenario, water is accreted during the formation phase of the terrestrial planets and not afterwards through bombardment as a late veneer. Typically, 50% of the water is accreted after the Earth has reached 60–70% of its final mass (*Morbidelli et al.*, 2012). This appears in contradiction with the measurements of the distinct D/H ratio in lunar water mentioned above, approximately twice that in the Earth's oceans (*Greenwood et al.*, 2011). If valid, this would indicate that a significant delivery of cometary water to the Earth-Moon system occurred shortly after the Moon-forming impact. The Earth water would thus be a late addition, resulting from only one, or at most a few collisions with the Earth that missed the Moon (*Robert*, 2011). Expanding the sample of objects with accurate D/H measurements is thus a high priority, long-term science goal for the new submillimeter facilities.

While the case for late delivery of water on Earth is still open, *Lunine et al.* (2003) showed that the abundance of water derived for early Mars is consistent with the general picture of late delivery by comets and bodies from the early asteroid belt. Unlike Earth, however, the small size of Mars dictates that it acquired its water primarily from very small bodies—asteroidal (sizes up to 100 km)—rather than lunar ($\sim$ 1700 km) or larger. The stochastic nature of the accretion process allows this to be one outcome out of many, but the Jupiter Grand Tack scenario provides a specific mechanism for removing larger bodies from the region where Mars formed, thereby resulting in its small size.

8.2.2. *Wet scenario*

There are two ways for Earth to get its water locally around 1 AU rather than through delivery from the outer solar system. The first option is that local planetesimals have retained some water at high temperatures through chemisorption onto silicate grains (*Drake*, 2005; *de Leeuw et al.*, 2010). There is no evidence for such material today in meteorites nor in the past in interstellar and protoplanetary dust (§ 5.1). However, the solid grains were bathed in abundant water vapor during the entire lifetime of gas-rich disks. This mechanism should differentiate between Earth and Venus. Computation and lab studies (*Stimpfl et al.*, 2006) suggest that chemisorption may be just marginally able to supply the inventory needed to explain Earth's crustal water, with some mantle water, but moving inward to 0.7 AU the efficiency of chemisorption should be significantly lower. Finding that Venus was significantly dryer than the Earth early in the solar system history would argue for the local wet source model, although such a model may also overpredict the amount of water acquired by Mars.

The second wet scenario is that Earth accretes a water rich atmosphere directly from the gas in the inner disk. This would require Earth to have had in the past a massive hydrogen atmosphere (with a molar ratio H_2/H_2O larger than 1) that experienced a slow hydrodynamical escape (*Ikoma and Genda*, 2006). One problem with this scenario is that the timescales for terrestrial planet formation are much longer than the lifetime of the gas disk. Also, the D/H ratio would be too low, unless photochemical processes at the disk surface enhance D/H in water and mix it down to the midplane (*Thi et al.*, 2010a) or over long timescales via mass-dependent atmospheric escape (*Genda and Ikoma*, 2008).

9. EXOPLANETARY ATMOSPHERES

H_2O is expected to be one of the dominant components in the atmospheres of giant exoplanets, so searches for signatures of water vapor started immediately when the field of transit spectroscopy with *Spitzer* opened up in 2007. Near-IR spectroscopy with HST and from the ground can be a powerful complement to these data because of the clean spectral features at 1–1.6 μm (Fig. 1). Early detections of water in HD 189733b, HD 209458 and XO1b were not uniformly accepted (see *Seager and Deming*, 2010; *Tinetti et al.*, 2012, and chapter by *Madhusudhan et al.* for summaries). Part of the problem may stem from hazes or clouds that can affect the spectra shortward of 1.5 μm and hide water which is visible at longer wavelengths. Even for the strongest cases for detection, it is difficult to retrieve an accurate water abundance profile from these data, because of the low S/N and low spectral resolution (*Madhusudhan and Seager*, 2010). The advent of a spatial scan mode has improved HST's ability to detect exoplanetary water with WFC3 (e.g., *Deming et al.*, 2013; *Mandell et al.*, 2013). New ground-based techniques are also yielding improved spectra (*Birkby et al.*, 2013), but dramatic improvements in sensitivity and wavelength range must await JWST. Until that time, only qualitative conclusions can be drawn.

9.1. Gas-giant planets

Models of hydrogen-dominated atmospheres of giant exoplanets ($T \approx 700 - 3000$ K; warm Neptune to hot Jupiter) solve for the molecular abundances (i.e., ratios of number densities, also called 'mixing ratios') under the assumption of thermochemical equilibrium. Non-equilibrium chemistry is important if transport (e.g., vertical mixing) is rapid enough that material moves out of a given temperature and pressure zone on a timescale short compared with that needed to reach equilibrium. The CH_4/CO ratio is most affected by such 'disequilibrium' chemistry, especially in the upper atmospheres. Since CO locks up some of the oxygen, this can also affect the H_2O abundance.

The two main parameters determining the water abundance profiles are the temperature-pressure combination

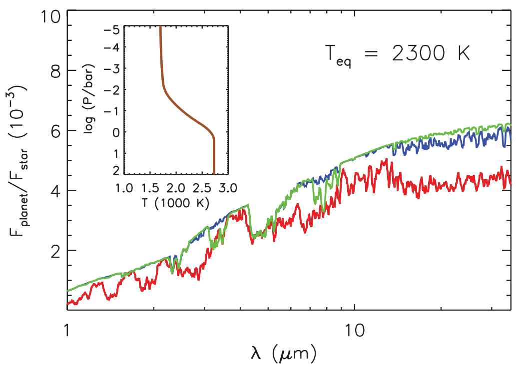

Fig. 13.— Spectra of the hot Jupiters with C/O ratios varying from 0.54 (solar, red) to 1 (blue) and 3 (green). Note the disappearance of the H_2O features at 1–3 μm as the C/O ratio increases. Figure from *Madhusudhan et al.* (2011b).

and the C/O ratio. Giant planets often show a temperature inversion in their atmospheres, with temperature increasing with height into the stratosphere, which affects both the abundances and the spectral appearance. However, for the full range of pressures (10^2–10^{-5} bar) and temperatures (700–3000 K), water is present at abundances greater than 10^{-3} with respect to H_2 for a solar C/O abundance ratio of 0.54, i.e., most of the oxygen is locked up in H_2O. In contrast, when the C/O ratio becomes close to unity or higher, the H_2O abundance can drop by orders of magnitude especially at lower pressures and higher temperatures, since the very stable CO molecule now locks up the bulk of the oxygen (*Kuchner and Seager*, 2005; *Madhusudhan et al.*, 2011b). CH_4 and other hydrocarbons are enhanced as well. As noted previously, observational evidence (not without controversy) for at least one case of such a carbon-rich giant planet, WASP-12b, has been found (*Madhusudhan et al.*, 2011a). Hot Jupiters like WASP-12b are easier targets for measuring C/O ratios, because their elevated temperature profiles allow both water and carbon-bearing species to be measured without the interference from condensation processes that hamper measurements in Jupiter and Saturn in our own solar system, although cloud-forming species more refractory than water ice can reduce spectral contrast for some temperature ranges. Figure 13 illustrates the changing spectral appearance with C/O ratio for a hot Jupiter ($T = 2300$ K); for cooler planets (< 1000 K) the changes are less obvious.

What can cause exoplanetary atmospheres to have very different C/O ratios from those found in the interstellar medium or even in their parent star? If giant planets indeed form outside the snow line at low temperatures through accretion of planetesimals, then the composition of the ices is a key ingredient in setting the C/O ratio. The volatiles (but not the rocky cores) vaporize when they enter the envelope of the planet and are mixed in the atmosphere during the homogenization process. As the giant planet migrates through the disk, it encounters different conditions and thus different ice compositions as a function of radius (*Mousis et al.*, 2009; *Öberg et al.*, 2011). Specifically a giant planet formed outside the CO snow line at 20–30 AU around a solar mass star may have a higher C/O ratio than that formed inside the CO (but outside the H_2O) snow line.

The exact composition of these planetesimals depends on the adopted model. The solar system community traditionally employs a model of the solar nebula disk, which starts hot and then cools off with time allowing various species to re-freeze. In this model, the abundance ratios of the ices are set by their thermodynamic properties ('condensation sequence') and the relative elemental abundances. For solar abundances, water is trapped in various clathrate hydrates like NH_3-H_2O and H_2S-5.75 H_2O between 5 and 20 AU. In a carbon-rich case, no water ice is formed and all the oxygen is CO, CO_2 and CH_3OH ice (*Madhusudhan et al.*, 2011b). The interstellar astrochemistry community, on the other hand, treats the entire disk with non-equilibrium chemistry, both with height and radius. Also, the heritage of gas and ice from the protostellar stage into the disk can be considered (*Aikawa and Herbst*, 1999; *Visser et al.*, 2009; *Aikawa et al.*, 2012; *Hincelin et al.*, 2013, see Fig. 5). The non-equilibrium models show that indeed the C/O ratio in ices can vary depending on location and differ by factors of 2–3 from the overall (stellar) abundances (*Öberg et al.*, 2011).

9.2. Rocky planets, super-Earths

The composition of Earth-like and super-Earth planets (up to 10 $M_\oplus$) is determined by similar thermodynamic arguments, with the difference that most of the material stays in solid form and no hydrogen-rich atmosphere is attracted. Well outside the snow line, at large distances from the parent star, the planets are built up largely from planetesimals that are half rock and half ice. If these planets move inward, the water can become liquid, resulting in 'ocean planets' or 'waterworlds', in which the entire surface of the planet is covered with water (*Kuchner*, 2003; *Léger et al.*, 2004). The oceans on such planets could be hundreds of kilometers deep and their atmospheres are likely thicker and warmer than on Earth because of the greenhouse effect of water vapor. Based on their relatively low bulk densities (from the mass-radius relation), the super-Earths GJ 1214b (*Charbonneau et al.*, 2009) and Kepler 22b (*Borucki et al.*, 2012) are candidate ocean planets.

Further examination of terrestrial planet models shows that there could be two types of water worlds: those which are true water rich in their bulk composition and those which are mostly rocky but have a significant fraction of their surface covered with water (Earth is in the latter category) (*Kaltenegger et al.*, 2013). Kepler 62e and f are prototypes of water-rich planets within the habitable zone, a category of planets that does not exist in our own solar system (*Borucki et al.*, 2013). Computing the atmospheric composition of terrestrial exoplanets is significantly more complex than that of giant exoplanets and requires consideration of many additional processes, including even plate tectonics (*Meadows and Seager*, 2011; *Fortney et al.*, 2013).

As for the terrestrial planets in our own solar system, the presence of one or more giant planet can strongly affect the amount of water on exo-(super)-Earths (Fig. 12). A wide variety of dynamical and population synthesis models on possible outcomes have been explored (e.g. *Raymond et al.*, 2006; *Mandell et al.*, 2007; *Bond et al.*, 2010; *Ida and Lin*, 2004, 2010; *Alibert et al.*, 2011; *Mordasini et al.*, 2009).

Water on a terrestrial planet in the habitable zone may be cycled many times between the liquid oceans and the atmosphere through evaporation and rain-out. However, only a very small fraction of water molecules are destroyed or formed over the lifetime of a planet like Earth. The total Earth hydrogen loss is estimated to be 3 kg s^{-1}. Even if all the hydrogen comes from photodissociation of water, the water loss would be 27 kg s^{-1}. Given the total mass of the hydrosphere of 1.5×10^{21} kg, it would take 1.8×10^{12} yr to deplete the water reservoir. The vast majority of the water bonds present today were, therefore, formed by the chemistry that led to the bulk of water in interstellar clouds and protoplanetary disks.

10. WATER TRAIL FROM CLOUDS TO PLANETS

Here we summarize the key points and list some outstanding questions.

- Water is formed on ice in dense molecular clouds. Some water is also formed in hot gas in shocks associated with protostars, but that water is largely lost to space.
- Water stays mostly as ice during protostellar collapse and infall. Only a small fraction of the gas in the inner envelope is in a 'hot core' where the water vapor abundance is high due to ice sublimation.
- Water enters the disk mostly as ice at large radii and is less affected by the accretion shock than previously thought.
- Water vapor is found in three different reservoirs in protoplanetary disks: the inner gaseous reservoir, the outer icy belt and the hot surface layers. The latter two reservoirs have now been observed with *Spitzer* and *Herschel* and quantified.
- Models suggest that the water that ends up in the planet and comet forming zones of disks is partly pristine ice and partly processed ice, i.e., ice that has at least once sublimated and recondensed when the material comes close to the young star.
- Water ice promotes grain growth to larger sizes; water-coated grains grow rapidly to planetesimal sizes in dust traps that have now been observed.
- Planetesimals inside the disk's snow line are expected to be dry, as found in our solar system. However, gaseous water can have very high abundances in the inner AU in the gas-rich phase. Some grains may have chemically bound water to silicates at higher

temperatures, but there is no evidence of hydrated silicates in meteorites nor in interstellar grains.

- Dynamics affects what type of planetesimals are available for planet formation in a certain location. The presence and migration of giant planets can cause scattering of water-rich planetesimals from the outer disk into the inner dry zone.
- Several comets have now been found with D/H ratios in water consistent with that of Earth's oceans. This helps to constrain models for the origin of water on the terrestrial planets, but does not yet give an unambiguous answer.
- Both dry and wet formation scenarios for Earth are still open, although most arguments favor accretion of water-rich planetesimals from the asteroid belt during the late stages of terrestrial planet formation. Delivery of water through bombardment to planetary surfaces in a 'late veneer' can contribute as well but may not have been dominant for Earth, in contrast with Mars.
- Jupiter may be poor in oxygen and water. If confirmed by the Juno mission to Jupiter, this may indicate a changing C/O ratio with disk radius. Evidence for this scenario comes from the detection of at least one carbon-rich exoplanet.
- All of the processes and key parameters identified here should also hold for exo-planetary systems.

There are a number of open questions that remain. A critical phase is the feeding of material from the collapsing core onto the disk, and the evolution of the young disk during the bulk of the phase of star formation. At present this phase has little observational constraints. In addition numerous models posit that viscous evolution and the relative movement of the dust to the gas can have impact on the overall water vapor evolution; this needs an observational basis. Astronomical observations have been confined to water vapor and ice emission from the disk surface but with the midplane hidden from view. What does this surface reservoir tells us about forming planets, both terrestrial and giant? Is there a way to detect the midplane, perhaps using HCO^+ (which is destroyed by water) as a probe of the snowline? However, this needs a source of ionization in the densest parts of the disk which may or may not be present (*Cleeves et al.*, 2013).

The exploration of deuterium enrichments continues to hold promise both in the solar system, with need for more information on the D/H values for water in the outer asteroids and (main belt) comets. It is also clear that we know less about the bulk elemental abundance of the solar system's largest reservoir of planetary material (i.e., Jupiter and Saturn) than one might have assumed. This must have implications for studies of extra-solar systems. In terms of the origin of the Earth's oceans matching the full range of geochemical constraints remains difficult.

Despite the uncertainties, there is a better understanding of the water trail from the clouds to planets. In this light, it is fascinating to consider that most of the water molecules in Earth's oceans and in our bodies may have been formed 4.6 billion years ago in the cloud out of which our solar system formed.

Acknowledgments. The authors thank many colleagues for collaborations and input, and various funding agencies for support, including NASA/JPL/Caltech. Figures by Magnus Persson, Ruud Visser, Lars Kristensen and Davide Fedele are much appreciated.

REFERENCES

Ádámkovics M. et al. (2013) *Astrophys. J.*, p. submitted.
Adriani A. et al. (2008) *Astrobiology*, *8*, 613.
A'Hearn M. F. (2011) *Annu. Rev. Astron. Astrophys.*, *49*, 281.
Aikawa Y. and Herbst E. (1999) *Astron. Astrophys.*, *351*, 233.
Aikawa Y. et al. (2012) *Astrophys. J.*, *760*, 40.
Akimkin V. et al. (2013) *Astrophys. J.*, *766*, 8.
Albertsson T. et al. (2014) *Astrophys. J.*, p. in press.
Alibert Y. et al. (2011) *Astron. Astrophys.*, *526*, A63.
Andersson S. and van Dishoeck E. F. (2008) *Astron. Astrophys.*, *491*, 907.
Arasa C. et al. (2010) *J. Chem. Phys.*, *132*, 18, 184510.
Atkinson R. et al. (2004) *Atmospheric chemistry and physics*, *4*, 1461.
Batalha N. M. et al. (2013) *Astrophys. J. Suppl.*, *204*, 24.
Bergin E. A. and van Dishoeck E. F. (2012) *Royal Society of London Philosophical Transactions Series A*, *370*, 2778.
Bergin E. A. et al. (2000) *Astrophys. J. Lett.*, *539*, L129.
Bergin E. A. et al. (2003) *Astrophys. J.*, *582*, 830.
Bergin E. A. et al. (2010) *Astron. Astrophys.*, *521*, L33.
Bethell T. J. and Bergin E. (2009) *Science*, *326*, 1675.
Bethell T. J. and Bergin E. A. (2011) *Astrophys. J.*, *739*, 78.
Birkby J. L. et al. (2013) *Mon. Not. R. Astron. Soc.*, *436*, L35.
Bisschop S. E. et al. (2007) *Astron. Astrophys.*, *465*, 913.
Bockelée-Morvan D. et al. (2012) *Astron. Astrophys.*, *544*, L15.
Bond J. C. et al. (2010) *Icarus*, *205*, 321.
Boogert A. C. A. et al. (2008) *Astrophys. J.*, *678*, 985.
Boogert A. C. A. et al. (2011) *Astrophys. J.*, *729*, 92.
Boonman A. M. S. and van Dishoeck E. F. (2003) *Astron. Astrophys.*, *403*, 1003.
Boonman A. M. S. et al. (2003) *Astron. Astrophys.*, *406*, 937.
Borucki W. J. et al. (2012) *Astrophys. J.*, *745*, 120.
Borucki W. J. et al. (2013) *Science*, *340*, 587.
Brown J. C. et al. (2011) *Astron. Astrophys.*, *535*, A71.
Bruderer S. et al. (2012) *Astron. Astrophys.*, *541*, A91.
Buhr H. et al. (2010) *Phys. Rev. Lett.*, *105*, 10.
Burke J. R. and Hollenbach D. J. (1983) *Astrophys. J.*, *265*, 223.
Bus S. J. and Binzel R. P. (2002) *Icarus*, *158*, 146.
Calvet N. et al. (1992) *Rev. Mex. Astron. Astrofis.*, *24*, 27.
Campins H. et al. (2010) *Nature*, *464*, 1320.
Carr J. S. and Najita J. R. (2008) *Science*, *319*, 1504.
Caselli P. et al. (2012) *Astrophys. J. Lett.*, *759*, L37.
Cavalié T. et al. (2013) *Astron. Astrophys.*, *553*, A21.
Cernicharo J. and Crovisier J. (2005) *Space Sci. Rev.*, *119*, 29.
Charbonneau D. et al. (2009) *Nature*, *462*, 891.
Cheung A. C. et al. (1969) *Nature*, *221*, 626.
Chiang E. I. and Goldreich P. (1997) *Astrophys. J.*, *490*, 368.
Chiang E. I. et al. (2001) *Astrophys. J.*, *547*, 1077.
Chiang H.-F. et al. (2008) *Astrophys. J.*, *680*, 474.
Ciesla F. J. and Cuzzi J. N. (2006) *Icarus*, *181*, 178.

Cleeves L. I. et al. (2013) *Astrophys. J.*, *777*, 28.
Coutens A. et al. (2012) *Astron. Astrophys.*, *539*, A132.
Coutens A. et al. (2013) *Astron. Astrophys.*, *560*, A39.
Crovisier J. et al. (2002) *Astron. Astrophys.*, *393*, 1053.
Cruikshank D. P. et al. (2000) *Icarus*, *147*, 309.
Cuppen H. M. et al. (2010) *PCCP*, *12*, 38, 12077.
Daniel F. et al. (2011) *Astron. Astrophys.*, *536*, A76.
Dartois E. et al. (2003) *Astron. Astrophys.*, *399*, 1009.
Davis S. S. (2007) *Astrophys. J.*, *660*, 1580.
de Leeuw N. H. et al. (2010) *Chem. Commun.*, *46*, 8923.
de Val-Borro M. et al. (2012) *Astron. Astrophys.*, *546*, L4.
Debes J. H. et al. (2013) *Astrophys. J.*, *771*, 45.
Deming D. et al. (2013) *Astrophys. J.*, *774*, 95.
Dodson-Robinson S. E. et al. (2009) *Icarus*, *200*, 672.
Dominik C. et al. (2005) *Astrophys. J. Lett.*, *635*, L85.
Donahue T. M. and Hodges Jr. R. R. (1992) *J. Geophys. Res.*, *97*, 6083.
Draine B. T. (1978) *Astrophys. J. Suppl.*, *36*, 595.
Drake M. J. (2005) *Meteoritics and Planetary Science*, *40*, 519.
Drossart P. et al. (1993) *Planet. Space Sci.*, *41*, 551.
Dulieu F. et al. (2013) *Nature Reports*, *3*, 1338.
Elitzur M. and Watson W. D. (1978) *Astrophys. J. Lett.*, *222*, L141.
Emprechtinger M. et al. (2013) *Astrophys. J.*, *765*, 61.
Encrenaz T. (2008) *Annu. Rev. Astron. Astrophys.*, *46*, 57.
Fedele D. et al. (2011) *Astrophys. J.*, *732*, 106.
Fedele D. et al. (2012) *Astron. Astrophys.*, *544*, L9.
Fedele D. et al. (2013) *Astron. Astrophys.*, *559*, A77.
Feuchtgruber H. et al. (1997) *Nature*, *389*, 159.
Feuchtgruber H. et al. (2013) *Astron. Astrophys.*, *551*, A126.
Flagey N. et al. (2013) *Astrophys. J.*, *762*, 11.
Fogel J. K. J. et al. (2011) *Astrophys. J.*, *726*, 29.
Fornasier S. et al. (2013) *Astron. Astrophys.*, *555*, A15.
Fortney J. J. et al. (2013) *Astrophys. J.*, *775*, 80.
Fraser H. J. et al. (2001) *Mon. Not. R. Astron. Soc.*, *327*, 1165.
Furuya K. et al. (2013) *Astrophys. J.*, *779*, 11.
Furuya R. S. et al. (2003) *Astrophys. J. Suppl.*, *144*, 71.
Genda H. and Ikoma M. (2008) *Icarus*, *194*, 42.
Gibb E. L. et al. (2004) *Astrophys. J. Suppl.*, *151*, 35.
Gillett F. C. and Forrest W. J. (1973) *Astrophys. J.*, *179*, 483.
Glassgold A. E. et al. (2009) *Astrophys. J.*, *701*, 142.
Gomes R. et al. (2005) *Nature*, *435*, 466.
Gorti U. et al. (2011) *Astrophys. J.*, *735*, 90.
Greenwood J. P. et al. (2011) *Nature Geoscience*, *4*, 79.
Gurwell M. A. et al. (2007) *Icarus*, *188*, 288.
Harsono D. et al. (2013) *Astron. Astrophys.*, *555*, A45.
Hartogh P. et al. (2011) *Nature*, *478*, 218.
Hayashi C. (1981) *Progr. Theor. Phys. Suppl.*, *70*, 35.
Heinzeller D. et al. (2011) *Astrophys. J.*, *731*, 115.
Herbst E. and Klemperer W. (1973) *Astrophys. J.*, *185*, 505.
Herbst E. and van Dishoeck E. F. (2009) *Annu. Rev. Astron. Astrophys.*, *47*, 427.
Herpin F. et al. (2012) *Astron. Astrophys.*, *542*, A76.
Hincelin U. et al. (2013) *Astrophys. J.*, *775*, 44.
Hogerheijde M. R. et al. (2011) *Science*, *334*, 338.
Hollenbach D. et al. (2009) *Astrophys. J.*, *690*, 1497.
Hollenbach D. et al. (2013) *Astrophys. J.*, *773*, 70.
Honda M. et al. (2009) *Astrophys. J. Lett.*, *690*, L110.
Horner J. et al. (2003) *Mon. Not. R. Astron. Soc.*, *343*, 1057.
Hsieh H. H. and Jewitt D. (2006) *Science*, *312*, 561.
Hsieh H. H. et al. (2004) *Astron. J.*, *127*, 2997.
Hudgins D. M. et al. (1993) *Astrophys. J. Suppl.*, *86*, 713.
Hutson M. and Ruzicka A. (2000) *Meteoritics and Planetary Science*, *35*, 601.
Ida S. and Lin D. N. C. (2004) *Astrophys. J.*, *616*, 567.
Ida S. and Lin D. N. C. (2010) *Astrophys. J.*, *719*, 810.
Ikoma M. and Genda H. (2006) *Astrophys. J.*, *648*, 696.
Ilee J. D. et al. (2011) *Mon. Not. R. Astron. Soc.*, *417*, 2950.
Indriolo N. and McCall B. J. (2012) *Astrophys. J.*, *745*, 91.
Jacquet E. and Robert F. (2013) *Icarus*, *223*, 722.
Janssen M. A. et al. (2005) *Icarus*, *173*, 447.
Jenniskens P. and Blake D. (1994) *Science*, *265*, 5173, 753.
Jewitt D. and Guilbert-Lepoutre A. (2012) *Astron. J.*, *143*, 21.
Johnson T. V. and Estrada P. R. (2009) in: *Saturn from Cassini-Huygens*, (edited by M. K. e. a. Dougherty), p. 55.
Jones T. D. et al. (1990) *Icarus*, *88*, 172.
Jonkheid B. et al. (2004) *Astron. Astrophys.*, *428*, 511.
Jørgensen J. K. and van Dishoeck E. F. (2010a) *Astrophys. J. Lett.*, *725*, L172.
Jørgensen J. K. and van Dishoeck E. F. (2010b) *Astrophys. J. Lett.*, *710*, L72.
Jørgensen J. K. et al. (2005) *Astrophys. J.*, *632*, 973.
Juhász A. et al. (2010) *Astrophys. J.*, *721*, 431.
Kaltenegger L. et al. (2013) *Astrophys. J. Lett.*, *775*, L47.
Kamp I. and Dullemond C. P. (2004) *Astrophys. J.*, *615*, 991.
Kamp I. et al. (2013) *Astron. Astrophys.*, *559*, A24.
Kaufman M. J. and Neufeld D. A. (1996) *Astrophys. J.*, *456*, 611.
Kennedy G. M. and Kenyon S. J. (2008) *Astrophys. J.*, *673*, 502.
Koike C. et al. (1982) *Astrophys. Space Sci.*, *88*, 89.
Kristensen L. E. et al. (2012) *Astron. Astrophys.*, *542*, A8.
Krot A. N. et al. (2000) *Protostars and Planets IV*, p. 1019.
Kuchner M. J. (2003) *Astrophys. J. Lett.*, *596*, L105.
Kuchner M. J. and Seager S. (2005) *arXiv:astro-ph/0504214*.
Küppers M. et al. (2005) *Nature*, *437*, 987.
Küppers M. et al. (2014) *Nature*, *505*, 525.
Lamberts T. et al. (2013) *PCCP*, *15*, 8287.
Lecacheux A. et al. (2003) *Astron. Astrophys.*, *402*, L55.
Lecar M. et al. (2006) *Astrophys. J.*, *640*, 1115.
Lécluse C. and Robert F. (1994) *Geochim. Cosmochim. Acta*, *58*, 2927.
Lécuyer C. et al. (1998) *Chem. Geol.*, *145*, 249.
Lefloch B. et al. (2010) *Astron. Astrophys.*, *518*, L113.
Léger A. et al. (2004) *Icarus*, *169*, 499.
Levison H. F. et al. (2010) *Science*, *329*, 187.
Licandro J. et al. (2011) *Astron. Astrophys.*, *532*, A65.
Lis D. C. et al. (2011) *Astrophys. J. Lett.*, *738*, L6.
Liu F.-C. et al. (2011) *Astron. Astrophys.*, *527*, A19.
Lodders K. (2004) *Astrophys. J.*, *611*, 587.
Lunine J. I. and Hunten D. M. (1987) *Icarus*, *69*, 566.
Lunine J. I. and Stevenson D. J. (1985) *Astrophys. J. Suppl.*, *58*, 493.
Lunine J. I. et al. (1991) *Icarus*, *94*, 333.
Lunine J. I. et al. (2003) *Icarus*, *165*, 1.
Madhusudhan N. and Seager S. (2010) *Astrophys. J.*, *725*, 261.
Madhusudhan N. et al. (2011a) *Nature*, *469*, 64.
Madhusudhan N. et al. (2011b) *Astrophys. J.*, *743*, 191.
Malfait K. et al. (1998) *Astron. Astrophys.*, *332*, L25.
Malfait K. et al. (1999) *Astron. Astrophys.*, *345*, 181.
Mandell A. M. et al. (2007) *Astrophys. J.*, *660*, 823.
Mandell A. M. et al. (2012) *Astrophys. J.*, *747*, 92.
Mandell A. M. et al. (2013) *Astrophys. J.*, *779*, 128.
Marty B. (2012) *Earth and Planetary Science Letters*, *313*, 56.
McClure M. K. et al. (2012) *Astrophys. J. Lett.*, *759*, L10.
Meadows V. and Seager S. (2011) in: *Exoplanets*, (edited by S. Seager), p. 441.

Meeus G. et al. (2012) *Astron. Astrophys.*, *544*, A78.
Meijerink R. et al. (2009) *Astrophys. J.*, *704*, 1471.
Melnick G. J. (2009) in: *Submillimeter Astrophysics and Technology*, vol. 417 of *ASP*, (edited by D. C. Lis et al.), p. 59.
Meyer D. M. et al. (1998) *Astrophys. J.*, *493*, 222.
Moore M. H. and Hudson R. L. (1994) *Astron. Astrophys. Suppl.*, *103*, 45.
Morbidelli A. et al. (2005) *Nature*, *435*, 462.
Morbidelli A. et al. (2012) *Annual Review of Earth and Planetary Sciences*, *40*, 251.
Mordasini C. et al. (2009) *Astron. Astrophys.*, *501*, 1139.
Mottram J. C. et al. (2013) *Astron. Astrophys.*, *558*, A126.
Mousis O. et al. (2009) *Astrophys. J.*, *696*, 1348.
Mousis O. et al. (2010) *Faraday Discussions*, *147*, 509.
Mousis O. et al. (2012) *Astrophys. J. Lett.*, *751*, L7.
Mumma M. J. and Charnley S. B. (2011) *Annu. Rev. Astron. Astrophys.*, *49*, 471.
Mumma M. J. et al. (1986) *Science*, *232*, 1523.
Murakawa K. et al. (2000) *Astrophys. J. Suppl.*, *128*, 603.
Najita J. R. et al. (2001) *Astrophys. J.*, *561*, 880.
Najita J. R. et al. (2011) *Astrophys. J.*, *743*, 147.
Neufeld D. A. and Hollenbach D. J. (1994) *Astrophys. J.*, *428*, 170.
Neufeld D. A. et al. (2000) *Astrophys. J. Lett.*, *539*, L151.
Neufeld D. A. et al. (2013) *Astrophys. J. Lett.*, *767*, L3.
Nisini B. et al. (2010) *Astron. Astrophys.*, *518*, L120.
Nomura H. et al. (2007) *Astrophys. J.*, *661*, 334.
Oba Y. et al. (2012) *Astrophys. J.*, *749*, 67.
Öberg K. I. et al. (2009) *Astrophys. J.*, *693*, 1209.
Öberg K. I. et al. (2011) *Astrophys. J.*, *740*, 109.
Olofsson J. et al. (2009) *Astron. Astrophys.*, *507*, 327.
Olofsson J. et al. (2012) *Astron. Astrophys.*, *542*, A90.
O'Rourke L. et al. (2013) *Astrophys. J. Lett.*, *774*, L13.
Owen T. and Bar-Nun A. (1993) *Nature*, *361*, 693.
Owen T. and Encrenaz T. (2006) *Planet. Space Sci.*, *54*, 1188.
Pagani L. et al. (1992) *Astron. Astrophys.*, *258*, 479.
Parise B. et al. (2003) *Astron. Astrophys.*, *410*, 897.
Persson M. V. et al. (2012) *Astron. Astrophys.*, *541*, A39.
Persson M. V. et al. (2013) *Astron. Astrophys.*, *549*, L3.
Podio L. et al. (2013) *Astrophys. J. Lett.*, *766*, L5.
Podolak M. and Zucker S. (2004) *Meteoritics and Planetary Science*, *39*, 1859.
Pontoppidan K. M. et al. (2004) *Astron. Astrophys.*, *426*, 925.
Pontoppidan K. M. et al. (2005) *Astrophys. J.*, *622*, 463.
Pontoppidan K. M. et al. (2010a) *Astrophys. J.*, *720*, 887.
Pontoppidan K. M. et al. (2010b) *Astrophys. J. Lett.*, *722*, L173.
Prasad S. S. and Tarafdar S. P. (1983) *Astrophys. J.*, *267*, 603.
Prinn R. G. and Fegley Jr. B. (1981) *Astrophys. J.*, *249*, 308.
Prodanović T. et al. (2010) *Mon. Not. R. Astron. Soc.*, *406*, 1108.
Przybilla N. et al. (2008) *Astrophys. J. Lett.*, *688*, L103.
Qi C. et al. (2013) *Science*, *341*, 630.
Raymond S. N. et al. (2006) *Science*, *313*, 1413.
Richet P. et al. (1977) *Annual Review of Earth and Planetary Sciences*, *5*, 65.
Rimmer P. B. et al. (2012) *Astron. Astrophys.*, *537*, A7.
Rivière-Marichalar P. et al. (2012) *Astron. Astrophys.*, *538*, L3.
Rivkin A. S. and Emery J. P. (2010) *Nature*, *464*, 1322.
Robert F. (2011) *Nature Geoscience*, *4*, 74.
Robert F. et al. (2000) *Space Sci. Rev.*, *92*, 201.
Roberts H. and Herbst E. (2002) *Astron. Astrophys.*, *395*, 233.
Roberts H. et al. (2003) *Astrophys. J. Lett.*, *591*, L41.
Roos-Serote M. et al. (2004) *Planet. Space Sci.*, *52*, 397.
Saal A. E. et al. (2013) *Science*, *340*, 6138, 1317.
Salyk C. et al. (2008) *Astrophys. J. Lett.*, *676*, L49.
Salyk C. et al. (2011) *Astrophys. J.*, *731*, 130.
Sasselov D. D. and Lecar M. (2000) *Astrophys. J.*, *528*, 995.
Schindhelm E. et al. (2012) *Astrophys. J. Lett.*, *756*, L23.
Schorghofer N. (2008) *Astrophys. J.*, *682*, 697.
Seager S. and Deming D. (2010) *Annu. Rev. Astron. Astrophys.*, *48*, 631.
Semenov D. and Wiebe D. (2011) *Astrophys. J. Suppl.*, *196*, 25.
Shimonishi T. et al. (2010) *Astron. Astrophys.*, *514*, A12.
Showman A. P. and Dowling T. E. (2000) *Science*, *289*, 1737.
Stevenson D. J. and Lunine J. I. (1988) *Icarus*, *75*, 146.
Stimpfl M. et al. (2006) *J. Cryst. Growth*, *294*, 1, 83.
Sultanov R. and Balakrishnan N. (2004) *J. Chem. Phys.*, *121*, 22, 11038.
Tafalla M. et al. (2013) *Astron. Astrophys.*, *551*, A116.
Taquet V. et al. (2013) *Astrophys. J. Lett.*, *768*, L29.
Terada H. et al. (2007) *Astrophys. J.*, *667*, 303.
Thi W. et al. (2010a) *Astron. Astrophys.*, *518*, L125.
Thi W.-F. et al. (2010b) *Mon. Not. R. Astron. Soc.*, *407*, 232.
Tielens A. G. G. M. (1983) *Astron. Astrophys.*, *119*, 177.
Tielens A. G. G. M. (2013) *Rev. Mod. Phys.*, *85*, 1021.
Tielens A. G. G. M. and Hagen W. (1982) *Astron. Astrophys.*, *114*, 245.
Tinetti G. et al. (2012) *Phil. Trans. Roy. Soc. A*, *370*, 1968, 2749.
Tsiganis K. et al. (2005) *Nature*, *435*, 459.
van der Marel N. et al. (2013) *Science*, *340*, 1199.
van Dishoeck E. et al. (2013) *Chemical Reviews*, *113*, 9043.
van Dishoeck E. F. et al. (2006) *Faraday Discussions*, *133*, 231.
van Dishoeck E. F. et al. (2011) *PASP*, *123*, 138.
van Zadelhoff G.-J. et al. (2003) *Astron. Astrophys.*, *397*, 789.
Vasyunin A. I. et al. (2011) *Astrophys. J.*, *727*, 76.
Visser R. et al. (2009) *Astron. Astrophys.*, *495*, 881.
Visser R. et al. (2011) *Astron. Astrophys.*, *534*, A132.
Visser R. et al. (2013) *Astrophys. J.*, *769*, 19.
Wallace L. et al. (1995) *Science*, *268*, 1155.
Walsh C. et al. (2012) *Astrophys. J.*, *747*, 114.
Walsh K. J. et al. (2011) *Nature*, *475*, 206.
Watson D. M. et al. (2007) *Nature*, *448*, 1026.
Watson D. M. et al. (2009) *Astrophys. J. Suppl.*, *180*, 84.
Weidenschilling S. J. and Cuzzi J. N. (1993) in: *Protostars and Planets III*, (edited by E. H. Levy and J. I. Lunine), p. 1031.
Weiß A. et al. (2013) *Astrophys. J.*, *767*, 88.
Westley M. S. et al. (1995) *Nature*, *373*, 405.
Whipple F. L. (1950) *Astrophys. J.*, *111*, 375.
Whittet D. C. B. (2010) *Astrophys. J.*, *710*, 1009.
Whittet D. C. B. et al. (1988) *Mon. Not. R. Astron. Soc.*, *233*, 321.
Whittet D. C. B. et al. (1998) *Astrophys. J. Lett.*, *498*, L159.
Whittet D. C. B. et al. (2013) *Astrophys. J.*, *774*, 102.
Willacy K. and Woods P. M. (2009) *Astrophys. J.*, *703*, 479.
Williams R. M. E. et al. (2013) *Science*, *340*, 1068.
Woitke P. et al. (2009a) *Astron. Astrophys.*, *501*, L5.
Woitke P. et al. (2009b) *Astron. Astrophys.*, *501*, 383.
Wong M. H. et al. (2008) in: *Oxygen in the Solar System*, vol. 68 of *Rev. Mineralogy & Geochem.*, (edited by G. e. a. MacPherson), p. 219.
Yang H. et al. (2012a) *Astrophys. J.*, *744*, 121.
Yang L. et al. (2012b) in: *Lunar and Planetary Inst. Sci. Conf. Abs.*, vol. 43, p. 2023.
Zasowski G. et al. (2009) *Astrophys. J.*, *694*, 459.
Zhang K. et al. (2013) *Astrophys. J.*, *766*, 82.

This 2-column preprint was prepared with the AAS LaTeX macros v5.2.